
The Unbalanced Gromov Wasserstein Distance: Conic Formulation and Relaxation

Thibault Séjourné
Ecole Normale Supérieure, DMA, PSL
thibault.sejourné@ens.fr

François-Xavier Vialard
Université Gustave Eiffel
francois-xavier.vialard@u-pem.fr

Gabriel Peyré
Ecole Normale Supérieure, DMA, CNRS, PSL
gabriel.peyre@ens.fr

Abstract

Comparing metric measure spaces (i.e. a metric space endowed with a probability distribution) is at the heart of many machine learning problems. The most popular distance between such metric measure spaces is the Gromov-Wasserstein (GW) distance, which is the solution of a quadratic assignment problem. The GW distance is however limited to the comparison of metric measure spaces endowed with a *probability* distribution. To alleviate this issue, we introduce two Unbalanced Gromov-Wasserstein formulations: a distance and a more tractable upper-bounding relaxation. They both allow the comparison of metric spaces equipped with arbitrary positive measures up to isometries. The first formulation is a positive and definite divergence based on a relaxation of the mass conservation constraint using a novel type of quadratically-homogeneous divergence. This divergence works hand in hand with the entropic regularization approach which is popular to solve large scale optimal transport problems. We show that the underlying non-convex optimization problem can be efficiently tackled using a highly parallelizable and GPU-friendly iterative scheme. The second formulation is a distance between mm-spaces up to isometries based on a conic lifting. Lastly, we provide numerical experiments on synthetic examples and domain adaptation data with a Positive-Unlabeled learning task to highlight the salient features of the unbalanced divergence and its potential applications in ML.

1 Introduction

Comparing data distributions on different metric spaces is a basic problem in machine learning. This class of problems is for instance at the heart of surfaces [Bronstein et al., 2006] or graph matching [Xu et al., 2019] (equipping the surface or graph with its associated geodesic distance), regression problems in quantum chemistry [Gilmer et al., 2017] (viewing the molecules as distributions of points in \mathbb{R}^3) and natural language processing [Grave et al., 2019, Alvarez-Melis and Jaakkola, 2018] (where texts in different languages are embedded as points distributions in different vector spaces).

Metric measure spaces. The mathematical way to formalize these problems is to model the data as *metric measure spaces* (mm-spaces). A mm-space is denoted as $\mathcal{X} = (X, d, \mu)$ where X is a complete separable set endowed with a distance d and a positive Borel measure $\mu \in \mathcal{M}_+(X)$. For instance, if $X = (x_i)_i$ is a finite set of points, then $\mu = \sum_i m_i \delta_{x_i}$ (here δ_{x_i} is the Dirac mass at x_i) is simply a set of positive weights $m_i = \mu(\{x_i\}) \geq 0$ associated to each point x_i , which accounts for its mass or importance. For instance, setting some m_i to 0 is equivalent to removing the point x_i . We

refer to Sturm [2012] for a mathematical account on the theory of mm-spaces. In all the applications highlighted above, it makes sense to perform the comparisons up to isometric transformations of the data. Two mm-spaces $\mathcal{X} = (X, d_X, \mu)$ and $\mathcal{Y} = (Y, d_Y, \nu)$ are considered to be equal (denoted $\mathcal{X} \sim \mathcal{Y}$) if they are isometric, meaning that there is a bijection $\psi : \text{spt}(\mu) \rightarrow \text{spt}(\nu)$ (where $\text{spt}(\mu)$ is the support of μ) such that $d_X(x, y) = d_Y(\psi(x), \psi(y))$ and $\psi_{\#}\mu = \nu$. Here $\psi_{\#}$ is the push-forward operator, so that $\psi_{\#}\mu = \nu$ is equivalent to imposing $\nu(A) = \mu(\psi^{-1}(A))$ for any set $A \subset Y$. For discrete spaces where $\mu = \sum_i m_i \delta_{x_i}$, then one should have $\nu = \psi_{\#}\mu = \sum_i m_i \delta_{\psi(x_i)}$. As highlighted by Mémoli [2011], considering mm-spaces up to isometry is a powerful way to formalize and analyze a wide variety of problems such as matching, regression and classification of distributions of points belonging to different spaces. Most often, the objects of interest come with a natural distance such as an intrinsic or extrinsic distance and the uniform measure is the usual choice to make mm-spaces widely applicable. The key to unlock all these problems is the computation of a distance between mm-spaces up to isometry. So far, existing distances (reviewed below) assume that μ is a probability distribution, i.e. $\mu(X) = 1$. This constraint is not natural and sometimes problematic for most of the practical applications to machine learning. The goal of this paper is to alleviate this restriction. We define for the first time a class of distances between unbalanced metric measure spaces, these distances being upper-bounded by divergences which can be approximated by an efficient numerical scheme.

Csiszár divergences The simplest case is when $X = Y$ and one simply ignores the underlying metric. One can then use Csiszár divergences (or φ -divergences), which perform a pointwise comparison (in contrast with optimal transport distances, which perform a displacement comparison). It is defined using an entropy function $\varphi : \mathbb{R}_+ \rightarrow [0, +\infty]$, which is a convex, lower semi-continuous, positive function with $\varphi(1) = 0$. The Csiszár φ -divergence reads $D_\varphi(\mu|\nu) \triangleq \int_X \varphi\left(\frac{d\mu}{d\nu}\right) d\nu + \varphi'_\infty \int_X d\mu^\perp$, where $\mu = \frac{d\mu}{d\nu}\nu + \mu^\perp$ is called the Radon-Nikodym or the Lebesgue decomposition of μ with respect to ν and $\varphi'_\infty = \lim_{r \rightarrow \infty} \varphi(r)/r \in \mathbb{R} \cup \{+\infty\}$ is called the recession constant. This divergence D_φ is convex, positive, 1-homogeneous and weak* lower-semicontinuous, see Liero et al. [2015] for details. Particular instances of φ -divergences are Kullback-Leibler (KL) for $\varphi(r) = r \log(r) - r + 1$ (note that $\varphi'_\infty = \infty$) and Total Variation (TV) for $\varphi(r) = |r - 1|$.

Balanced and unbalanced optimal transport. If the common embedding space X is equipped with a distance $d(x, y)$, one can use more elaborated methods such as optimal transport (OT) distances, which are computed by solving convex optimization problems. This type of methods has proven useful for ML problems as diverse as domain adaptation [Courty et al., 2014], supervised learning over histograms [Frogner et al., 2015] and unsupervised learning of generative models [Arjovsky et al., 2017]. In this case, the extension from probability distributions to arbitrary positive measures $(\mu, \nu) \in \mathcal{M}_+(X)^2$ is now well understood and corresponds to the theory of unbalanced OT. Following Liero et al. [2015], Chizat et al. [2018a], a family of unbalanced Wasserstein distances is defined by solving

$$\text{UW}(\mu, \nu)^q \triangleq \inf_{\pi \in \mathcal{M}(X \times X)} \int \lambda(d(x, y)) d\pi(x, y) + D_\varphi(\pi_1|\mu) + D_\varphi(\pi_2|\nu). \quad (1)$$

Here (π_1, π_2) are the two marginals of the joint distribution π , defined by $\pi_1(A) = \pi(A \times Y)$ for $A \subset X$. The mapping $\lambda : \mathbb{R}^+ \rightarrow \mathbb{R}$ and exponent $q \geq 1$ should be chosen wisely to ensure for instance that UW defines a distance (see Section 2.2.1). It is frequent to take ρD_φ instead of D_φ (i.e. take $\psi = \rho\varphi$) to adjust the strength of the marginals' penalization. Balanced OT is retrieved with the convex indicator $\varphi = \iota_{\{1\}}$ (i.e. $\varphi(1) = 0$ and $\varphi(x) = +\infty$ otherwise) or by taking the limit $\rho \rightarrow +\infty$, which enforces $\pi_1 = \mu$ and $\pi_2 = \nu$. When $0 < \rho < +\infty$, unbalanced OT operates a trade-off between transportation and creation of mass, which is crucial to be robust to outliers in the data and to cope with mass variations in the modes of the distributions. For supervised tasks, the value of ρ should be cross-validated to obtain the best performances. Its use is gaining popularity in applications, such as medical imaging registration [Feydy et al., 2019a], videos [Lee et al., 2019], generative learning [Balaji et al., 2020] and gradient flow to train neural networks [Chizat and Bach, 2018, Rotskoff et al., 2019]. Furthermore, existing efficient algorithms for balanced OT extend to this unbalanced problem. In particular Sinkhorn's iterations, introduced in ML for balanced OT by Cuturi [2013], extend to unbalanced OT [Chizat et al., 2018b, Séjourné et al., 2019], as detailed in Section 3.

The Gromov-Wasserstein distance and its applications. The Gromov-Wasserstein (GW) distance [Mémoli, 2011, Sturm, 2012] generalizes the notion of OT to the setting of mm-spaces up to

isometries. It replaces the linear cost $\int \lambda(d)d\pi$ of OT by a quadratic function. It reads

$$\text{GW}(\mathcal{X}, \mathcal{Y})^q \triangleq \min_{\pi \in \mathcal{M}_+(X \times Y)} \left\{ \int \lambda(|d_X(x, x') - d_Y(y, y')|)d\pi(x, y)d\pi(x', y') : \begin{matrix} \pi_1 = \mu \\ \pi_2 = \nu \end{matrix} \right\}. \quad (2)$$

It is proved in Mémoli [2011], Sturm [2012] that GW defines with $\lambda(t) = t^q$ a distance up to isometries on balanced mm-spaces (i.e. the measures are probability distributions). The GW distance is applied successfully in natural language processing for unsupervised translation learning [Grave et al., 2019, Alvarez-Melis and Jaakkola, 2018], in generative learning for objects lying in spaces of different dimensions [Bunne et al., 2019] and to build VAE for graphs [Xu et al., 2020]. It has been adapted for domain adaptation over different spaces [Redko et al., 2020]. It is also a relevant distance to compute barycenters between graphs or shapes [Vayer et al., 2018, Chowdhury and Needham, 2020]. When $(\mathcal{X}, \mathcal{Y})$ are Euclidean spaces, this distance compares distributions up to rigid isometry, and is closely related (but not equal) to metrics defined by procrustes analysis [Grave et al., 2019, Alvarez-Melis et al., 2019]. The problem (2) is non convex because the quadratic form $\int \lambda(|d_X - d_Y|)d\pi \otimes \pi$ is not positive in general. It is in fact closely related to quadratic assignment problems [Burkard et al., 1998], which are used for graph matching problems, and are known to be NP-hard in general. Nevertheless, non-convex optimization methods have been shown to be successful in practice to use GW distances for ML problems. This includes for instance alternating minimization [Mémoli, 2011, Redko et al., 2020] and entropic regularization [Peyré et al., 2016, Gold and Rangarajan, 1996].

Related works and contributions. The concomitant work of De Ponti and Mondino [2020] extends the L^p transportation distance defined in Sturm et al. [2006] to unbalanced mm-spaces and studies its geometric properties. This distortion distance is not equivalent to the GW distance, and is more difficult to estimate numerically because it explicitly imposes a triangle inequality constraint in the optimization problem. The work of Chapel et al. [2020] relaxes the GW distance to the unbalanced setting by hybridizing GW with partial OT [Figalli, 2010] for unsupervised labeling. It resembles one particular setting of our formulation, but with some important differences, detailed in Section 2. Our construction is also connected to partial matching methods, which find numerous applications in graphics and vision [Cosmo et al., 2016]. In particular, Rodola et al. [2012] introduces a mass conservation relaxation of the GW problem.

The two main contributions of this paper are the definition of two formulations relaxing the GW distance. The first one is called the Unbalanced Gromov-Wasserstein (UGW) divergence and can be computed efficiently on GPUs. The second one is called the Conic Gromov-Wasserstein distance (CGW). It is proved to be a distance between mm-spaces endowed with positive measures up to isometries, as stated in Theorem 1 which is the main theoretical result of this paper. We also prove in Theorem 1 that UGW can be used as a surrogate upper-bounding CGW. We present those concepts and their properties in Section 2. We also detail in Section 3 an efficient computational scheme for a particular setting of UGW. This method computes an approximate stationary point of a biconvex relaxation of our formulations. Even though it is a lower bound of the original problem, we provide in Theorem 3 conditions ensuring the tightness of this relaxation in many cases of interest. The algorithm leverages the strength of entropic regularization and the Sinkhorn algorithm, namely that it is GPU-friendly and defines smooth loss functions amenable to back-propagation for ML applications. Section 4 provides some numerical experiments to highlight the qualitative behavior of this algorithm and its ability to cope with outliers and mass variations in the modes of the distributions. We illustrate numerically the tightness of the relation between UGW and CGW, showing that UGW is a reasonable proxy of a distance, at least locally. We provide an application of our divergence in the positive unlabeled learning setting, using domain adaptation data, and display results which are at par or outperform the computable competitor Chapel et al. [2020].

2 Unbalanced Gromov-Wasserstein formulations

We present in this section our two new formulations and their properties. The first one, called UGW, is exploited in Sections 3 and 4 to derive an efficient algorithm used in numerical experiments. The second one, called CGW, defines a distance between mm-spaces up to isometries. Those results build upon the work of Liero et al. [2015], and a summary of the construction of UOT is detailed in Appendix A. In all what follows, we consider complete separable mm-spaces endowed with a metric and a positive measure.

2.1 The unbalanced Gromov-Wasserstein divergence

This new formulation makes use of quadratic φ -divergences, defined as $D_\varphi^\otimes(\rho|\nu) \triangleq D_\varphi(\rho \otimes \rho|\nu \otimes \nu)$, where $\rho \otimes \rho \in \mathcal{M}_+(X^2)$ is the tensor product measure defined by $d(\rho \otimes \rho)(x, y) = d\rho(x)d\rho(y)$. Note that D_φ^\otimes is not a convex function in general.

Definition 1 (Unbalanced GW). *The Unbalanced Gromov-Wasserstein divergence is defined as* $UGW(\mathcal{X}, \mathcal{Y}) = \inf_{\pi \in \mathcal{M}_+(X \times Y)} \mathcal{L}(\pi) \triangleq \mathcal{G}(\pi) + D_\varphi^\otimes(\pi_1|\mu) + D_\varphi^\otimes(\pi_2|\nu)$.

This definition can be understood as an hybridation between (1) and (2) but with a twist: one needs to use the quadratic divergence D_φ^\otimes in place of D_φ . To the best of our knowledge, it is the first time such quadratic divergences are being used and studied. In the TV case, this is the most important distinction between UGW and partial-GW [Chapel et al., 2020]. Note also that the balanced GW distance (2) is recovered as a particular case when using $\varphi = \iota_{\{1\}}$ or by letting $\rho \rightarrow +\infty$ for an entropy $\psi = \rho\varphi$.

Using quadratic divergences results in UGW being 2-homogeneous: for $\theta \geq 0$, writing $(\mathcal{X}_\theta, \mathcal{Y}_\theta)$ equipped with $(\theta\mu, \theta\nu)$, one has $\theta^{-2}UGW(\mathcal{X}_\theta, \mathcal{Y}_\theta) = UGW(\mathcal{X}, \mathcal{Y})$. When using non tensorized φ -divergences, the resulting unbalanced Gromov-Wasserstein functional between \mathcal{X}_θ and \mathcal{Y}_θ have very different and inconsistent behaviors when $\theta \rightarrow 0$ and $\theta \rightarrow +\infty$. Indeed, once normalized by θ^{-2} and θ^{-1} , one obtains respectively balanced GW and a Hellinger-type distance. Using tensorized divergences ensures that the behavior does not depends on θ . It is also fundamental to connect UGW with our distance CGW, see Theorem 1 and Appendix B.

We first prove the existence of optimal plans π minimizing \mathcal{L} , which holds for the three key settings of Section 2.2.1, namely for KL, TV, and for compact metric spaces (such as finite pointclouds and graphs). All proofs are deferred in Appendix B.

Proposition 1 (Existence of minimizers). *We assume that (X, Y) are compact and that either (i) φ superlinear, i.e $\varphi'_\infty = \infty$, or (ii) λ has compact sublevel sets in \mathbb{R}_+ and $2\varphi'_\infty + \inf \lambda > 0$. Then there exists $\pi \in \mathcal{M}_+(X \times Y)$ such that $UGW(\mathcal{X}, \mathcal{Y}) = \mathcal{L}(\pi)$.*

The following proposition ensures that the functional UGW can be used to compare mm-spaces.

Proposition 2 (Definiteness of UGW). *Assume that $\varphi^{-1}(\{0\}) = \{1\}$ and $\lambda^{-1}(\{0\}) = \{0\}$. Then $UGW(\mathcal{X}, \mathcal{Y}) \geq 0$ and is 0 if and only if $\mathcal{X} \sim \mathcal{Y}$.*

We end this section with a reformulation of UGW which is important to make the connection with the second formulation CGW of the following section. It splits UGW into two parts: the term $\varphi(0)(|(\mu \otimes \mu)^\perp| + |(\nu \otimes \nu)^\perp|)$ accounts for the pure creation/destruction of mass and a new transport cost L_c accounts for the remaining part (partial/pure transport and partial creation/destruction of mass).

Lemma 1. *Defining $L_c(a, b) \triangleq c + a\varphi(1/a) + b\varphi(1/b)$, and writing $(f \triangleq \frac{d\mu}{d\pi_1}, g \triangleq \frac{d\nu}{d\pi_2})$ the Lebesgue densities of (μ, ν) w.r.t. (π_1, π_2) such that $\mu = f\pi_1 + \mu^\perp$ and $\nu = g\pi_2 + \nu^\perp$, one has*

$$\mathcal{L}(\pi) = \int_{X^2 \times Y^2} L_{\lambda(|d_X - d_Y|)}(f \otimes f, g \otimes g) d\pi d\pi + \varphi(0)(|(\mu \otimes \mu)^\perp| + |(\nu \otimes \nu)^\perp|). \quad (3)$$

Proof. Write $f = \frac{d\mu}{d\pi_1}$ and $g = \frac{d\nu}{d\pi_2}$. The Lebesgue decompositions read $\mu \otimes \mu = (f \otimes f)\pi_1 \otimes \pi_1 + (\mu \otimes \mu)^\perp$ and $\nu \otimes \nu = (g \otimes g)\pi_2 \otimes \pi_2 + (\nu \otimes \nu)^\perp$, thanks to the tensorized structure of the decomposed plans. To prove Equation (3), we need to define the reverse entropy Liero et al. [2015] such that $D_\varphi(\alpha|\mu) = D_\psi(\mu|\alpha)$, where $\psi(x) \triangleq x\varphi(\frac{1}{x})$ is also an entropy function satisfying $\psi'_\infty = \varphi(0)$. One then has

$$\begin{aligned} \mathcal{L}(\pi) &= \int_{X^2 \times Y^2} \lambda(\Gamma) d\pi d\pi + D_\varphi^\otimes(\pi_1|\mu) + D_\varphi^\otimes(\pi_2|\nu) \\ &= \int_{X^2 \times Y^2} \lambda(\Gamma) d\pi d\pi + D_\psi^\otimes(\mu|\pi_1) + D_\psi^\otimes(\nu|\pi_2) \end{aligned}$$

$$\begin{aligned}
\mathcal{L}(\pi) &= \int_{X^2 \times Y^2} \lambda(\Gamma) d\pi d\pi + \int_{X^2} \psi(f \otimes f) d\pi_1 d\pi_1 + \int_{Y^2} \psi(g \otimes g) d\pi_2 d\pi_2 \\
&\quad + \varphi(0)(|(\mu \otimes \mu)^\perp| + |(\nu \otimes \nu)^\perp|) \\
&= \int_{X^2 \times Y^2} L_{\lambda(\Gamma)}(f \otimes f, g \otimes g) d\pi d\pi + \varphi(0)(|(\mu \otimes \mu)^\perp| + |(\nu \otimes \nu)^\perp|).
\end{aligned}$$

Using the definition of ψ in L_c ends the proof. \square

2.2 The conic Gromov-Wasserstein distance

We introduce a second ‘‘conic’’ formulation of unbalanced GW, which is connected to UGW, and whose construction is inspired by the conic formulation of UOT (see Appendix A for an overview).

2.2.1 Background on cone sets and distances

The conic formulation lifts a point $x \in X$ to a couple $(x, r) \in X \times \mathbb{R}^+$ where r encodes some (power of a) mass. Then we seek optimal transport plans defined over $\mathfrak{C}[X] \triangleq X \times \mathbb{R}_+ / (X \times \{0\})$, where coordinates $(x, r = 0)$ with no mass are merged into a single point \mathfrak{o}_X called the apex of the cone. In the sequel, points of $X \times \mathbb{R}_+$ are noted (x, r) , while $[x, r]$ are quotiented points of $\mathfrak{C}[X]$.

While transport plans depend on variables $([x, r], [y, s])$ and $([x', r'], [y', s'])$ in $\mathfrak{C}[X] \times \mathfrak{C}[Y]$, the transportation cost involved in our conic formulation only makes use of the 2-D cone $\mathfrak{C}[\mathbb{R}_+]$ over \mathbb{R}_+ endowed with the distance $|u - v|$ (note that any other distance on \mathbb{R} could be used as well). More specifically, we consider coordinates of the form $([u, a], [v, b]) = ([d_X(x, x'), rr'], [d_Y(y, y'), ss']) \in \mathfrak{C}[\mathbb{R}_+] \times \mathfrak{C}[\mathbb{R}_+]$. Thus we now describe conic discrepancies \mathcal{D} on $\mathfrak{C}[\mathbb{R}_+]$, which are defined for $(p, q) \geq 1$ as $\mathcal{D}([u, a], [v, b])^q \triangleq H_{\lambda(|u-v|)}(a^p, b^p)$, where $H_c(a^p, b^p) \triangleq \inf_{\theta \geq 0} \theta L_c(\frac{a^p}{\theta}, \frac{b^p}{\theta})$ is the perspective transform of L_c introduced in Lemma 1. The intuition underpinning the definition of this cost is that the perspective transform accounts for the possibility to rescale a transport plan π by a scalar θ but the scaling is performed pointwise instead of globally. In general \mathcal{D} is not a distance, but it is always definite as stated by this result proved in Appendix A.

Proposition 3. *Assume $\lambda^{-1}(\{0\}) = \{0\}$, $\varphi^{-1}(\{0\}) = \{1\}$ and φ is coercive. Then \mathcal{D} is definite on $\mathfrak{C}[\mathbb{R}_+]$, i.e. $\mathcal{D}([u, a], [v, b]) = 0$ if and only if $(a = b = 0)$ or $(a = b \text{ and } u = v)$.*

Of particular interest are those φ where \mathcal{D} is a distance, which necessitates a careful choice of λ, p and q . We now detail three examples where this is the case.

Gaussian Hellinger distance (GH). When $D_\varphi = \text{KL}$, $\lambda(t) = t^2$ and $q = p = 2$, then one has $\mathcal{D}([u, a], [v, b])^2 = a^2 + b^2 - 2abe^{-|u-v|/2}$. This cone distance [Burago et al., 2001] is further generalized by De Ponti [2019] who shows that \mathcal{D} is a distance for power entropies $\varphi(s) = \frac{s^p - p(s-1) - 1}{p(p-1)}$ if $p \geq 1$ (the case $p = 1$ corresponding to $D_\varphi = \text{KL}$).

Hellinger-Kantorovich (HK) / Wasserstein-Fisher-Rao distance (WFR). When $D_\varphi = \text{KL}$, $\lambda(t) = -\log \cos^2(t \wedge \frac{\pi}{2})$ and $q = p = 2$, then one has $\mathcal{D}([u, a], [v, b])^2 = a^2 + b^2 - 2ab \cos(\frac{\pi}{2} \wedge |u - v|)$. This construction, which might seem peculiar, corresponds to the one used to make unbalanced OT a geodesic distance, as detailed in [Liero et al., 2015, Chizat et al., 2018a].

Partial optimal transport distance (PT). When $D_\varphi = \text{TV}$, $\lambda(t) = t^q$, $q \geq 1$ and $p = 1$, then $\mathcal{D}([u, a], [v, b])^q = a + b - (a \wedge b)(2 - |u - v|^q)_+$ defines a cone distance [Chizat et al., 2018a].

2.2.2 Definitions and properties

The conic formulation consists in solving a GW problem on the cone, with the addition of two linear constraints. Informally speaking, L_c from Lemma 1 becomes \mathcal{D} , the term $(|(\mu \otimes \mu)^\perp| + |(\nu \otimes \nu)^\perp|)$ is taken into account by the constraints (5) below, and the variables (f, g) are replaced by (r^p, s^p) . It reads $\text{CGW}(\mathcal{X}, \mathcal{Y}) \triangleq \inf_{\alpha \in \mathcal{U}_p(\mu, \nu)} \mathcal{H}(\alpha)$ where

$$\mathcal{H}(\alpha) \triangleq \int \mathcal{D}([d_X(x, x'), rr'], [d_Y(y, y'), ss'])^q d\alpha([x, r], [y, s]) d\alpha([x', r'], [y', s']), \quad (4)$$

and $\mathcal{U}_p(\mu, \nu)$ is defined as the set

$$\mathcal{U}_p(\mu, \nu) \triangleq \left\{ \alpha \in \mathcal{M}_+(\mathfrak{C}[X] \times \mathfrak{C}[Y]), \int_{\mathbb{R}_+} r^p d\alpha_1(\cdot, r) = \mu, \int_{\mathbb{R}_+} s^p d\alpha_2(\cdot, s) = \nu \right\}. \quad (5)$$

It is similar to the conic formulation of UW, see Appendix A. Note that similarly to the GW formulation (2) – and in sharp contrast with the conic formulation of UW – here the transport plans are defined on the cone $\mathcal{C}[X] \times \mathcal{C}[Y]$ but the cost \mathcal{D} is a distance on $\mathcal{C}[\mathbb{R}_+]$.

We present now the main contributions of this paper, proved in Appendix C. We state that CGW defines a distance under conditions that hold for the settings of Section 2.2.1, and that it is upper-bounded by UGW. The divergence UGW can be approximated with efficient numerical schemes as detailed in Section 3.

Theorem 1. (i) *The divergence CGW is symmetric, positive and definite up to isometries. (ii) If \mathcal{D} is a distance on $\mathcal{C}[\mathbb{R}_+]$, then $\text{CGW}^{1/q}$ is a distance on the set of mm-spaces up to isometries. (iii) For any $(D_\varphi, \lambda, p, q)$ with associated cost \mathcal{D} on the cone, one has $\text{UGW} \geq \text{CGW}$.*

3 Algorithms

We focus in this section on the numerical computation of the upper bound UGW using a bi-convex relaxation and derive an alternate minimization scheme coupled with entropic regularization. We also propose to approximate CGW by doing a similar alternate minimization, as detailed in Appendix E. We provide guarantees of tightness on the bi-convex relaxation for CGW (see Theorem 3). The computation of the distance CGW is heavy in practice because it requires an optimization over a lifted conic space, which needs to be discretized. Thus it does not scale to large problem for CGW, but allows to explore numerically how tight is the upper bound $\text{UGW} \geq \text{CGW}$, see Section 4. The algorithm for UGW is presented on arbitrary measures, the special case of discrete measures being a particular case. The discretized formulas and algorithms are detailed in Appendix D, see also Chizat et al. [2018b], Peyré et al. [2016]. All implementations are available at https://github.com/thibsej/unbalanced_gromov_wasserstein, and installable in Python with the command `pip install unbalancedgw`.

3.1 Bi-convex relaxation and tightness

In order to derive a simple numerical approximation scheme, following Mémoli [2011], we introduce a lower bound obtained by introducing two transportation plans. To further accelerate the method and enable GPU-friendly iterations, similarly to Gold et al. [1996], Solomon et al. [2016], we consider an entropic regularization. It reads, for any $\varepsilon \geq 0$,

$$\begin{aligned} \text{UGW}_\varepsilon(\mathcal{X}, \mathcal{Y}) &\triangleq \inf_{\pi} \mathcal{L}(\pi) + \varepsilon \text{KL}^\otimes(\pi | \mu \otimes \nu) \geq \inf_{\pi, \gamma} \mathcal{F}(\pi, \gamma) + \varepsilon \text{KL}(\pi \otimes \gamma | (\mu \otimes \nu)^{\otimes 2}), \quad (6) \\ \text{and } \mathcal{F}(\pi, \gamma) &\triangleq \int_{X^2 \times Y^2} \lambda(|d_X - d_Y|) d\pi \otimes \gamma + D_\varphi(\pi_1 \otimes \gamma_1 | \mu \otimes \mu) + D_\varphi(\pi_2 \otimes \gamma_2 | \nu \otimes \nu), \end{aligned}$$

where (γ_1, γ_2) denote the marginals of the plan γ . In the sequel we write $\mathcal{F}_\varepsilon = \mathcal{F} + \varepsilon \text{KL}^\otimes$. Note that in contrast to the entropic regularization of GW Peyré et al. [2016], here we use a tensorized entropy to maintain the overall homogeneity of the energy. A simple method to approximate this lower bound is to perform an alternate minimization on π and γ , which is known to converge for smooth φ to a stationary point since the coupling term in the functional is smooth [Tseng, 2001]. Note that if $\pi \otimes \gamma$ is optimal then so is $(s\pi) \otimes (\frac{1}{s}\gamma)$ with $s \geq 0$. Thus without loss of generality we can optimize under the constraint $m(\pi) = m(\gamma)$ by setting $s = \sqrt{m(\gamma)/m(\pi)}$.

We now discuss the tightness of the bi-convex relaxation by generalizing a result of Konno. We first present a result which applies to general quadratic assignment problems, then state its application to our setting.

Theorem 2 (Tight relaxation). *Let B a Banach space, let $f : B \mapsto \mathbb{R} \cup \{+\infty\}$ be a function and let $\mathcal{L} : C \subset B \mapsto \mathbb{R}$ the function defined on the convex set $C \subset B$ by $\mathcal{L}(\pi) = \frac{1}{2} \langle \pi, k(\pi) \rangle + 2f(\pi)$ where k is a symmetric bilinear map which is negative (not necessarily definite) on $\Delta C \triangleq \text{Span}\{\pi - \gamma; (\pi, \gamma) \in C\}$, that is, for any $z \in \Delta C$, $\langle z, kz \rangle \leq 0$. Assume that there exists $\pi_0 \in C$ such that $\mathcal{L}(\pi_0) < +\infty$, and define $\mathcal{F}(\pi, \gamma) \triangleq \frac{1}{2} \langle \pi, k(\gamma) \rangle + f(\pi) + f(\gamma)$. Then, for any $(\pi_*, \gamma_*) \in \arg \min \mathcal{F}(\pi, \gamma)$, we have $\mathcal{F}(\pi_*, \pi_*) = \mathcal{F}(\gamma_*, \gamma_*) = \mathcal{F}(\pi_*, \gamma_*)$. Moreover, if one assumes either that k is a definite kernel or f is strictly convex, one gets $\pi_* = \gamma_*$.*

The above Theorem 2 is proved in Appendix D. As an application, we now state our tightness result for GW_ε and CGW. In those settings the optimizers of the bi-convex relaxation are also optimal for the original problem.

Theorem 3. *For GW_ε with $\varepsilon \geq 0$ or for CGW, assume that $\lambda(t) = t^2$ and that (d_X, d_Y) are both conditionnally negative (or conditionally positive) kernels. Then the bi-convex relaxation of both problems is tight.*

Proof. The proof for CGW is detailed in Appendix E, we prove the tightness for GW_ε . When $\lambda(t) = t^2$ the kernel $k = \lambda(|d_X - d_Y|)$ is conditionally negative on the set $\{(\pi, \gamma), \pi_1 = \gamma_1 \text{ and } \pi_2 = \gamma_2\}$, i.e. we have $\langle (\pi - \gamma), k(\pi - \gamma) \rangle \leq 0$ (see Maron and Lipman [2018]). For GW_ε one has $\pi_1 = \gamma_1 = \mu$ and $\pi_2 = \gamma_2 = \nu$ thanks to the constraints on marginals. Thus the kernel is negative semi-definite and the proof of Theorem 2 applies, hence the tightness of the relaxation. \square

Konno’s result Konno [1976] applies for unregularized ($\varepsilon = 0$), Balanced-GW. The novelty of Theorem 3 is its extension to both GW_ε and CGW. So far it is an open question whether the relaxation is tight or not for UGW_ε , because the above proof no longer holds. Note that in all our numerical simulations, our solvers always found solutions of UGW_ε such that $\pi = \gamma$ when $|d_X - d_Y|^2$ is conditionally negative. The property that the kernel $|d_X - d_Y|^2$ is negative does not hold in general (e.g. for graph geodesic distances) and the tightness of the relaxation remains open in this setting. We know from [Maron and Lipman, 2018, Theorem 1] that it is conditionally negative semi-definite when both (d_X, d_Y) are conditionally negative kernels. Examples of distances which are negative kernels are tree metrics in the case of graphs, as well as Euclidean, spherical and hyperbolic distances over their respective manifolds Feragen et al. [2015]. In practice, when ε is small, we observed in the indefinite setting that the relaxation outputs more frequently spurious minima than in the negative semi-definite setting.

3.2 Alternate Sinkhorn minimization

Minimizing the lower bound (6) with respect to either π or γ is non-trivial for an arbitrary φ . We restrict our attention to the Kullback-Leibler case $D_\varphi = \rho\text{KL}$ with $\rho > 0$, which can be addressed by solving a regularized and convex unbalanced problem as studied in Chizat et al. [2018b], Séjourné et al. [2019]. It is explained in the following proposition.

Proposition 4. *For a fixed γ , the optimal $\pi \in \arg \min_{\pi} \mathcal{F}(\pi, \gamma) + \varepsilon\text{KL}(\pi \otimes \gamma | (\mu \otimes \nu)^{\otimes 2})$ solves*

$$\min_{\pi} \int c_{\gamma}^{\varepsilon}(x, y) d\pi(x, y) + \rho m(\gamma) \text{KL}(\pi_1 | \mu) + \rho m(\gamma) \text{KL}(\pi_2 | \nu) + \varepsilon m(\gamma) \text{KL}(\pi | \mu \otimes \nu),$$

where $m(\gamma) \triangleq \gamma(X \times Y)$ is the mass of γ , and where we define the cost associated to γ as

$$c_{\gamma}^{\varepsilon}(x, y) \triangleq \int \lambda(|d_X(x, \cdot) - d_Y(y, \cdot)|) d\gamma + \rho \int \log\left(\frac{d\gamma_1}{d\mu}\right) d\gamma_1 + \rho \int \log\left(\frac{d\gamma_2}{d\nu}\right) d\gamma_2 + \varepsilon \int \log\left(\frac{d\gamma}{d\mu d\nu}\right) d\gamma.$$

Computing the cost c_{γ}^{ε} for spaces X and Y of n points has in general a cost $O(n^4)$ in time and memory. However, as explained for instance in Peyré et al. [2016], for the special case $\lambda(t) = t^2$, this cost is reduced to $O(n^3)$ in time and $O(n^2)$ in memory. This is the setting we consider in the numerical simulations. This makes the method applicable for scales of the order of 10^4 points. For larger datasets one should use approximation schemes such as hierarchical approaches [Xu et al., 2019] or Nyström compression of the kernel [Altschuler et al., 2018].

The resulting alternate minimization method is detailed in Algorithm 1, see Appendix D for a discretized version. It uses the unbalanced Sinkhorn algorithm of Chizat et al. [2018b], Séjourné et al. [2019] as sub-iterations and takes $\pi = \mu \otimes \nu / \sqrt{m(\mu)m(\nu)}$ to initialize the updates. This Sinkhorn algorithm operates over a pair of continuous functions (so-called

Algorithm 1 – $\text{UGW}(\mathcal{X}, \mathcal{Y}, \rho, \varepsilon)$

Input: mm-spaces $(\mathcal{X}, \mathcal{Y})$, relax. ρ , regul. ε

Output: π, γ solving (6)

Init. $\pi = \gamma = \mu \otimes \nu / \sqrt{m(\mu)m(\nu)}$, $g = 0$.

while (π, γ) has not converged **do**

 Update $\pi \leftarrow \gamma$,

 then $c \leftarrow c_{\pi}^{\varepsilon}$, $\tilde{\rho} \leftarrow m(\pi)\rho$, $\tilde{\varepsilon} \leftarrow m(\pi)\varepsilon$

while (f, g) has not converged **do**

$f \leftarrow -\frac{\tilde{\varepsilon}\tilde{\rho}}{\tilde{\varepsilon}+\tilde{\rho}} \log \int e^{(g(y)-c(\cdot, y))/\tilde{\varepsilon}} d\nu(y)$

$g \leftarrow -\frac{\tilde{\varepsilon}\tilde{\rho}}{\tilde{\varepsilon}+\tilde{\rho}} \log \int e^{(f(x)-c(x, \cdot))/\tilde{\varepsilon}} d\mu(x)$

end while

 Upd. $\gamma(x, y) \leftarrow e^{\frac{f(x)+g(y)-c(x, y)}{\tilde{\varepsilon}}} \mu(x)\nu(y)$

 Rescale $\gamma \leftarrow \sqrt{m(\pi)/m(\gamma)}\gamma$

end while

Return (π, γ) .

Kantorovitch potentials) $f(x)$ and $g(y)$. For discrete spaces X and Y of size n , these functions are stored in vectors of size n , and that integral involved in the updates becomes a sum. Each iteration of Sinkhorn thus has a cost n^2 , and all the involved operation can be efficiently mapped to parallelizable GPU routines as detailed in Chizat et al. [2018b], Séjourné et al. [2019]. Another advantage of using an unbalanced Sinkhorn algorithm is its complexity $O(n^2/\varepsilon)$ to compute an ε -approximation, as stated in Pham et al. [2020], which should be compared to $O(n^2/\varepsilon^2)$ operations for balanced Sinkhorn.

Note also that balanced GW is recovered as a special case when setting $\rho \rightarrow +\infty$, so that $\tilde{\rho}/(\tilde{\varepsilon} + \tilde{\rho}) \rightarrow 1$ should be used in the iterations. In order to speed up Sinkhorn inner-loops, especially for small values of ε , one can use linear extrapolation [Thibault et al., 2017] or non-linear Anderson acceleration [Anderson, 1965, Scieur et al., 2016].

There is an extra scaling step after computing γ involving the mass $m(\pi)$. It corresponds to the scaling s of $\pi \otimes \gamma$ such that $m(\pi) = m(\gamma)$, and we observe that this scaling is key not only to impose this mass equality but also to stabilize the algorithm. Otherwise we observed that $m(\gamma) < 1 < m(\pi)$ and underflows whenever $m(\gamma) \rightarrow 0$ and $m(\pi) \rightarrow \infty$.

4 Numerical experiments

This section presents simulations on synthetic examples to highlight the qualitative behavior of UGW and the tightness of the bound $UGW \geq CGW$. Other illustrations on UGW are available in Appendix E. We end the section with a learning application of UGW in a positive-unlabeled setting, using domain adaptation data so as to compare with PGW Chapel et al. [2020]. In the synthetic experiments, μ and ν are probability distributions, which allows us to compare GW with UGW.

Robustness to imbalanced classes. In this first example, we take $X = \mathbb{R}^3$, $Y = \mathbb{R}^2$ and consider \mathcal{E}_2 , \mathcal{E}_3 , \mathcal{C} and \mathcal{S} to be uniform distributions on a 2D and 3D ellipse, a square and a sphere. We consider mm-spaces of different dimensions to emphasize the ability of (U)GW to compare different spaces. Figure 1 contrasts the transportation plan obtained by GW and UGW for a fixed $\mu = 0.5\mathcal{E}_3 + 0.5\mathcal{S}$ and ν obtained using two different mixtures of \mathcal{E}_2 and \mathcal{C} . The black segments show the largest entries of the transportation matrix π , for a sub-sampled set of points (to ease visibility), thus effectively displaying the matching induced by the plan. Furthermore, the width of the dots are scaled according to the mass of the marginals $\pi_1 \approx \mu$ and $\pi_2 \approx \nu$, i.e. the smaller the point, the smaller is the amount of transported mass. This figure shows that the exact conservation of mass imposed by GW leads to a poor geometrical matching of the shapes which have different global mass. As this should be expected, UGW recovers coherent matchings. We suspect the alternate minimization algorithm is able to find the global minimum in these cases.

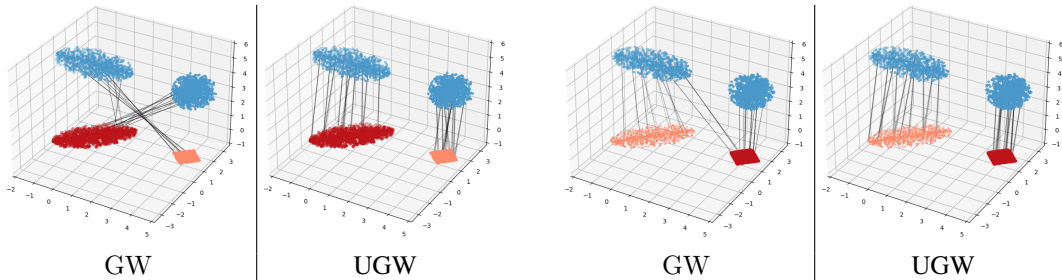


Figure 1: GW vs. UGW transportation plan, using $\nu = 0.3\mathcal{E}_2 + 0.7\mathcal{C}$ on the left, and $\nu = 0.7\mathcal{E}_2 + 0.3\mathcal{C}$ on the right. The 2D mm-spaces is lifted into \mathbb{R}^3 by padding the third coordinate to zero.

Tightness of the bound $CGW \leq UGW$ We propose to approximate CGW by doing a similar alternate minimization as for UGW, as detailed in Appendix E. This numerical scheme does not scale to large problems, but allows us to explore numerically how tight is the upper bound $UGW \geq CGW$. Figure 2 highlights the fact that in Euclidean space $X = Y = \mathbb{R}^d$, this bound seems to be tight when the two measures are sufficiently close. We consider discrete measures $\mu = \frac{1}{n} \sum_i \delta_{x_i}$ in $X = Y = \mathbb{R}^d$ and $\nu_t = \frac{1}{n} \sum_i \delta_{y_i}$ where $y_i = x_i + t\Delta_i$ where Δ_i are random perturbations and

denote $(\mathcal{X}, \mathcal{Y}_t)$ the two mm-spaces associated to the Euclidean distance. As $t \rightarrow 0$, μ and ν_t get closer, we observe numerically that $UGW \approx CGW$. Figure 3 considers random points $(x_i)_i$ and $(y_i)_i$ and displays the histograms of the ratio CGW/UGW for $n = 3$. This shows that while the bound $CGW \leq UGW$ seems not tight, the ratio appears to be bounded even for points not being close. This numerical experiment suggests that UGW and CGW are locally equivalent and that UGW is in practice an acceptable proxy of the distance CGW . We leave for future works a tighter analysis of the gap between UGW and CGW .

Positive unlabeled learning experiments Positive Unlabeled (PU) learning is a semi-supervised classification problem, where instead of learning from positive and negative samples $(x_i, \ell_i)_i$ with labels $\ell_i \in \{-1, 1\}$ we only learn from one class labeled with positives, i.e. only those $X \triangleq \{x_i : \ell_i = 1\}$. The task is to leverage X to predict the classes $\ell = \ell(y) \in \{-1, +1\}$ of unlabelled $y \in Y$ belong to a separate space. We consider here that X, Y are embedded in Euclidean space, and denote \mathcal{X}, \mathcal{Y} the associated labelled and unlabelled mm-spaces, equipped with the uniform distribution. Our experiments are adapted from Partial-GW (PGW) Chapel et al. [2020], which used partial GW to solve PU-learning. The rationale of using unbalanced OT methods for PU learning stems from the fact that positive samples should be matched with positive due to their similar features, while negative samples would be ignored due to dissimilar features that induce a laziness to transport mass and match them.

We consider PU learning over the Caltech office dataset used for domain adaptation tasks (with domains Caltech (C) Griffin et al. [2007], Amazon (A), Webcam (W) and DSLR (D) Saenko et al. [2010]). The Caltech datasets are represented with two embeddings based on Surf and Decaf features Saenko et al. [2010], Donahue et al. [2014]. On the latter datasets, we perform PU learning over similar features (e.g. surf-C \rightarrow surf-* or decaf-C \rightarrow decaf-*) and from one feature format to the other (e.g. surf-C \rightarrow decaf-* or surf-C \rightarrow decaf-*). Those features are projected via PCA to subspaces of dimension 10 for surf features and 40 for decaf features. In the last task, one cannot use standard PU-method, and to the best of our knowledge, Unbalanced-GW methods are the only approaches for PU learning across different domains/features.

The procedure is the following. We solve the PU learning problem by computing the optimal plan π for $UGW(\mathcal{X}, \mathcal{Y})$. We compute its first marginal π_2 on \mathcal{Y} , and predict the labels of some $y \in Y$ as $\ell(y) \triangleq \text{sign}(\pi_2(y) - q)$ where q is the quantile of π_2 corresponding to the proportion r of positives samples in Y . Following Chapel et al. [2020] which is adapted from Kato et al. [2018], Hsieh et al. [2019], this proportion r is assumed to be known. We report the accuracy of the prediction over the same 20 folds of the datasets, and use 20 other folds to validate the parameters of UGW . We consider 100 random samples for each fold of (X, Y) , a ratio of positive samples $r = 0.1$ for domains (C,A,W,D), and a ratio $r = 0.2$ for domains (C,A,W).

Since the GW objective is non-convex, the initialization of the minimization algorithms is key to obtain good performances. In Chapel et al. [2020] and our experiments, for tasks where X and Y belong to the same Euclidean space, (e.g. surf-C \rightarrow surf-*) we initialize π with the Partial-Wasserstein (PW) solution with a squared Euclidean cost. For cross-domain prediction (e.g. surf-C \rightarrow decaf-*), following Chapel et al. [2020], PGW is initialized with a list of plans built using a coarsened representation of the data with k -NN. While Chapel et al. [2020] makes use in an oracle manner of the plan providing the best accuracy, we modified their protocol and keep the plan which has the lowest PGW cost, which seems fairer, hence the difference in performance with Chapel et al. [2020]. To initialize UGW when X and Y do not belong to the same Euclidean space, we use a UOT solution of a matching between distance

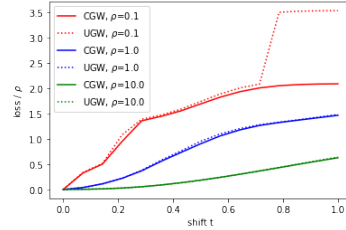


Figure 2: Comparison of $UGW(\mathcal{X}, \mathcal{Y}_t)$ and $CGW(\mathcal{X}, \mathcal{Y}_t)$ as the support gets shifted by a perturbation.

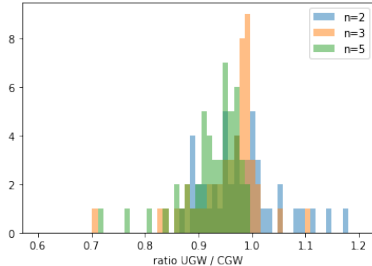


Figure 3: Histograms of the ratio CGW/UGW for random spaces with $n \in \{2, 3, 5\}$ samples. Ratios over 1 are due to local minima.

Dataset	prior	Init (PW)	PGW	UGW	Dataset	prior	Init (FLB)	PGW	UGW
surf-C → surf-C	0.1	89.9	84.9	83.9	surf-C → decaf-C	0.1	85.0	85.1	85.6
surf-C → surf-A	0.1	81.8	82.2	83.5	surf-C → decaf-A	0.1	84.2	87.1	83.6
surf-C → surf-W	0.1	81.9	81.3	80.3	surf-C → decaf-W	0.1	86.2	88.6	86.8
surf-C → surf-D	0.1	80.0	81.4	83.2	surf-C → decaf-D	0.1	84.7	91.1	90.7
surf-C → surf-C	0.2	79.7	75.7	75.4	surf-C → decaf-C	0.2	74.8	75.6	75.9
surf-C → surf-A	0.2	65.6	66.0	76.4	surf-C → decaf-A	0.2	76.2	87.9	82.4
surf-C → surf-W	0.2	65.1	64.3	67.3	surf-C → decaf-W	0.2	81.5	88.4	89.9
decaf-C → decaf-C	0.1	93.9	83.0	86.8	decaf-C → surf-C	0.1	81.7	81.0	81.1
decaf-C → decaf-A	0.1	80.1	81.4	85.6	decaf-C → surf-A	0.1	80.9	81.2	82.4
decaf-C → decaf-W	0.1	80.1	82.7	86.1	decaf-C → surf-W	0.1	82.0	81.3	83.5
decaf-C → decaf-D	0.1	80.6	83.8	83.4	decaf-C → surf-D	0.1	80.0	80.8	81.5
decaf-C → decaf-C	0.2	90.6	76.7	80.5	decaf-C → surf-C	0.2	66.6	63.7	65.2
decaf-C → decaf-A	0.2	62.5	68.7	74.7	decaf-C → surf-A	0.2	62.9	62.4	69.3
decaf-C → decaf-W	0.2	65.7	75.9	79.2	decaf-C → surf-W	0.2	65.1	61.4	83.3

Table 1: Accuracy for all tasks. The left block are domain adaptation experiments with similar features, where both PGW and UGW are initialised with PW. The right block are domain adaptation experiments with different features, and the reported init is FLB (see Appendix E) used for UGW.

histograms called FLB Mémoli [2011]. We define FLB in our UGW setting as

$$\text{FLB}(\mathcal{X}, \mathcal{Y}) \triangleq \min \int_{\mathcal{X} \times \mathcal{Y}} |\bar{\mu} \star d_X - \bar{\nu} \star d_Y|^2 d\pi + \rho \text{KL}(\pi_1 | \mu) + \rho \text{KL}(\pi_2 | \nu) + \varepsilon \text{KL}(\pi | \mu \otimes \nu), \quad (7)$$

where $\mu \star d_X(x) \triangleq \int d_X(x, x') d\mu(x')$ is the eccentricity, i.e. a histogram of aggregated distances, and $\bar{\mu} = \mu/m(\mu)$. Contrary to GW Mémoli [2011], there is a priori no link between FLB and UGW.

In the experiments we slightly generalize UGW and use two different marginal penalties $\rho_1 \text{KL}^\otimes(\pi_1 | \mu) + \rho_2 \text{KL}^\otimes(\pi_2 | \nu)$ with two parameters (ρ_1, ρ_2) to take into account shifts between domains/features. Note that PGW has a single parameter (which plays a role similar to (ρ_1, ρ_2)) which controls the cost of mass creation/destruction. We set $\varepsilon = 2^{-9}$, which avoids introducing an extra parameter in the method. The value $(\rho_1, \rho_2) \in \{2^{-k}, k \in \llbracket 5, 10 \rrbracket\}^2$ are cross validated for each task on the validation folds, and we report the average accuracy on the testing folds. We discuss in Appendix E the impact of reducing the number of parameters on the performance. Comparison with other methods – PU and PUSB Kato et al. [2018], Du Plessis et al. [2014] – are provided in Chapel et al. [2020] and we focus here on the comparison with PGW only.

The results are reported in Table 1. We display the performance of PGW, UGW and the initialization used for UGW to guarantee that using UGW does improve the performance. We observe that when the source and target dataset is the same (C→C tasks), the PW initialization performs better and PGW/UGW degrade the performance, so that in this setting Optimal Transport should be preferred over GW, which is to be expected. However when the domains are different, applying UGW improves the performance over the initialization (which is FLB) in almost all tasks. Note that in that case the methods PU, PUSB or PW cannot be used. Overall, this shows that GW methods are able to solve to some extent the PU learning problem across different spaces, and that using a “softer” KL penalties in UGW is at least at par with Partial GW, and performs better in some settings.

5 Conclusion and perspectives

This paper defines two Unbalanced Gromov-Wasserstein formulations: CGW and UGW. We prove that they are both positive and definite. We provide a scalable, GPU-friendly algorithm to compute UGW illustrate its applicability in learning tasks, and show that CGW is a distance between mm-spaces up to isometry. These divergences and distances allow for the first time to blend in a seamless way the transportation geometry of GW with creation and destruction of mass. This hybridization is the key to unlock both theoretical and practical issues. This work opens new questions for future works, for instance removing the bias introduced by the use of entropic regularization, which is important for applications to ML. Note that such a debiasing was successfully applied for Balanced-GW in Bunne et al. [2019] and is shown to lead to a valid divergence for balanced OT in Feydy et al. [2019b] and UW in Séjourné et al. [2019]. The design of efficient numerical solvers for CGW is also an interesting avenue for future works, as well as the study of its induced topology.

Acknowledgements

The works of Thibault Séjourné and Gabriel Peyré is supported by the ERC grant NORIA. The work of G. Peyré was supported in part by the French government under management of Agence Nationale de la Recherche as part of the "Investissements d'avenir" program, reference ANR19-P3IA-0001 (PRAIRIE 3IA Institute).

The authors thank Rémi Flamary for his remarks and advices, as well as Laetitia Chapel for her help to reproduce her experiments.

References

- Alexander M Bronstein, Michael M Bronstein, and Ron Kimmel. Generalized multidimensional scaling: a framework for isometry-invariant partial surface matching. *Proceedings of the National Academy of Sciences*, 103(5):1168–1172, 2006.
- Hongteng Xu, Dixin Luo, and Lawrence Carin. Scalable gromov-wasserstein learning for graph partitioning and matching. In *Advances in neural information processing systems*, pages 3046–3056, 2019.
- Justin Gilmer, Samuel S Schoenholz, Patrick F Riley, Oriol Vinyals, and George E Dahl. Neural message passing for quantum chemistry. In *Proceedings of the 34th International Conference on Machine Learning-Volume 70*, pages 1263–1272. JMLR. org, 2017.
- Edouard Grave, Armand Joulin, and Quentin Berthet. Unsupervised alignment of embeddings with wasserstein procrustes. In *The 22nd International Conference on Artificial Intelligence and Statistics*, pages 1880–1890, 2019.
- David Alvarez-Melis and Tommi S Jaakkola. Gromov-wasserstein alignment of word embedding spaces. *arXiv preprint arXiv:1809.00013*, 2018.
- Karl-Theodor Sturm. The space of spaces: curvature bounds and gradient flows on the space of metric measure spaces. *arXiv preprint arXiv:1208.0434*, 2012.
- Facundo Mémoli. Gromov–wasserstein distances and the metric approach to object matching. *Foundations of computational mathematics*, 11(4):417–487, 2011.
- Matthias Liero, Alexander Mielke, and Giuseppe Savaré. Optimal entropy-transport problems and a new hellinger–kantorovich distance between positive measures. *Inventiones mathematicae*, pages 1–149, 2015.
- Nicolas Courty, Rémi Flamary, and Devis Tuia. Domain adaptation with regularized optimal transport. In *Joint European Conference on Machine Learning and Knowledge Discovery in Databases*, pages 274–289. Springer, 2014.
- Charlie Frogner, Chiyuan Zhang, Hossein Mobahi, Mauricio Araya, and Tomaso A Poggio. Learning with a Wasserstein loss. In *Advances in Neural Information Processing Systems*, pages 2053–2061, 2015.
- Martin Arjovsky, Soumith Chintala, and Léon Bottou. Wasserstein GAN. *arXiv preprint arXiv:1701.07875*, 2017.
- Lénaïc Chizat, Gabriel Peyré, Bernhard Schmitzer, and François-Xavier Vialard. Unbalanced optimal transport: Dynamic and kantorovich formulations. *Journal of Functional Analysis*, 274(11): 3090–3123, 2018a.
- Jean Feydy, Pierre Roussillon, Alain Trounev, and Pietro Gori. Fast and scalable optimal transport for brain tractograms. In *International Conference on Medical Image Computing and Computer-Assisted Intervention*, pages 636–644. Springer, 2019a.
- John Lee, Nicholas P Bertrand, and Christopher J Rozell. Parallel unbalanced optimal transport regularization for large scale imaging problems. *arXiv preprint arXiv:1909.00149*, 2019.

- Yogesh Balaji, Rama Chellappa, and Soheil Feizi. Robust optimal transport with applications in generative modeling and domain adaptation. *Advances in Neural Information Processing Systems*, 33, 2020.
- Lenaïc Chizat and Francis Bach. On the global convergence of gradient descent for over-parameterized models using optimal transport. In *Advances in neural information processing systems*, pages 3036–3046, 2018.
- Grant Rotskoff, Samy Jelassi, Joan Bruna, and Eric Vanden-Eijnden. Global convergence of neuron birth-death dynamics. *arXiv preprint arXiv:1902.01843*, 2019.
- Marco Cuturi. Sinkhorn distances: Lightspeed computation of optimal transport. In *Adv. in Neural Information Processing Systems*, pages 2292–2300, 2013.
- Lenaïc Chizat, Gabriel Peyré, Bernhard Schmitzer, and François-Xavier Vialard. Scaling algorithms for unbalanced transport problems. *to appear in Mathematics of Computation*, 2018b.
- Thibault Séjourné, Jean Feydy, François-Xavier Vialard, Alain Trounev, and Gabriel Peyré. Sinkhorn divergences for unbalanced optimal transport. *arXiv preprint arXiv:1910.12958*, 2019.
- Charlotte Bunne, David Alvarez-Melis, Andreas Krause, and Stefanie Jegelka. Learning generative models across incomparable spaces. *arXiv preprint arXiv:1905.05461*, 2019.
- Hongteng Xu, Dixin Luo, Ricardo Henao, Svati Shah, and Lawrence Carin. Learning autoencoders with relational regularization. *arXiv preprint arXiv:2002.02913*, 2020.
- Ivegen Redko, Titouan Vayer, Rémi Flamary, and Nicolas Courty. Co-optimal transport. *arXiv preprint arXiv:2002.03731*, 2020.
- Titouan Vayer, Laetitia Chapel, Rémi Flamary, Romain Tavenard, and Nicolas Courty. Fused gromov-wasserstein distance for structured objects: theoretical foundations and mathematical properties. *arXiv preprint arXiv:1811.02834*, 2018.
- Samir Chowdhury and Tom Needham. Gromov-wasserstein averaging in a riemannian framework. In *Proceedings of the IEEE/CVF Conference on Computer Vision and Pattern Recognition Workshops*, pages 842–843, 2020.
- David Alvarez-Melis, Stefanie Jegelka, and Tommi S Jaakkola. Towards optimal transport with global invariances. In *The 22nd International Conference on Artificial Intelligence and Statistics*, pages 1870–1879. PMLR, 2019.
- Rainer E Burkard, Eranda Cela, Panos M Pardalos, and Leonidas S Pitsoulis. The quadratic assignment problem. In *Handbook of combinatorial optimization*, pages 1713–1809. Springer, 1998.
- Gabriel Peyré, Marco Cuturi, and Justin Solomon. Gromov-wasserstein averaging of kernel and distance matrices. In *International Conference on Machine Learning*, pages 2664–2672, 2016.
- Steven Gold and Anand Rangarajan. A graduated assignment algorithm for graph matching. *IEEE Transactions on pattern analysis and machine intelligence*, 18(4):377–388, 1996.
- Nicoló De Ponti and Andrea Mondino. Entropy-transport distances between unbalanced metric measure spaces. *arXiv preprint arXiv:2009.10636*, 2020.
- Karl-Theodor Sturm et al. On the geometry of metric measure spaces. *Acta mathematica*, 196(1): 65–131, 2006.
- Laetitia Chapel, Mokhtar Z Alaya, and Gilles Gasso. Partial gromov-wasserstein with applications on positive-unlabeled learning. *arXiv preprint arXiv:2002.08276*, 2020.
- Alessio Figalli. The optimal partial transport problem. *Archive for rational mechanics and analysis*, 195(2):533–560, 2010.
- Luca Cosmo, Emanuele Rodolà, Michael M Bronstein, Andrea Torsello, Daniel Cremers, and Y Sahillioglu. Shrec’16: Partial matching of deformable shapes. *Proc. 3DOR*, 2(9):12, 2016.

- Emanuele Rodola, Alex M Bronstein, Andrea Albarelli, Filippo Bergamasco, and Andrea Torsello. A game-theoretic approach to deformable shape matching. In *2012 IEEE Conference on Computer Vision and Pattern Recognition*, pages 182–189. IEEE, 2012.
- Dmitri Burago, Iu D Burago, Yuri Burago, Sergei A Ivanov, and Sergei Ivanov. *A course in metric geometry*, volume 33. American Mathematical Soc., 2001.
- Nicolò De Ponti. Metric properties of homogeneous and spatially inhomogeneous f -divergences. *IEEE Transactions on Information Theory*, 66(5):2872–2890, 2019.
- Steven Gold, Anand Rangarajan, et al. Softmax to softassign: Neural network algorithms for combinatorial optimization. *Journal of Artificial Neural Networks*, 2(4):381–399, 1996.
- J. Solomon, G. Peyré, V. Kim, and S. Sra. Entropic metric alignment for correspondence problems. *ACM Transactions on Graphics (TOG)*, 35(4), 2016.
- Paul Tseng. Convergence of a block coordinate descent method for nondifferentiable minimization. *Journal of optimization theory and applications*, 109(3):475–494, 2001.
- Haggai Maron and Yaron Lipman. (probably) concave graph matching. *arXiv preprint arXiv:1807.09722*, 2018.
- Hiroshi Konno. Maximization of a convex quadratic function under linear constraints. *Mathematical programming*, 11(1):117–127, 1976.
- Aasa Feragen, Francois Lauze, and Soren Hauberg. Geodesic exponential kernels: When curvature and linearity conflict. In *Proceedings of the IEEE Conference on Computer Vision and Pattern Recognition*, pages 3032–3042, 2015.
- Jason Altschuler, Francis Bach, Alessandro Rudi, and Jonathan Weed. Massively scalable Sinkhorn distances via the nyström method. *arXiv preprint arXiv:1812.05189*, 2018.
- Khiem Pham, Khang Le, Nhat Ho, Tung Pham, and Hung Bui. On unbalanced optimal transport: An analysis of sinkhorn algorithm. *arXiv preprint arXiv:2002.03293*, 2020.
- Alexis Thibault, Lénaïc Chizat, Charles Dossal, and Nicolas Papadakis. Overrelaxed Sinkhorn-Knopp algorithm for regularized optimal transport. *arXiv preprint arXiv:1711.01851*, 2017.
- Donald G Anderson. Iterative procedures for nonlinear integral equations. *Journal of the ACM (JACM)*, 12(4):547–560, 1965.
- Damien Scieur, Alexandre d’Aspremont, and Francis Bach. Regularized nonlinear acceleration. In *Advances In Neural Information Processing Systems*, pages 712–720, 2016.
- Gregory Griffin, Alex Holub, and Pietro Perona. Caltech-256 object category dataset. 2007.
- Kate Saenko, Brian Kulis, Mario Fritz, and Trevor Darrell. Adapting visual category models to new domains. In *European conference on computer vision*, pages 213–226. Springer, 2010.
- Jeff Donahue, Yangqing Jia, Oriol Vinyals, Judy Hoffman, Ning Zhang, Eric Tzeng, and Trevor Darrell. Decaf: A deep convolutional activation feature for generic visual recognition. In *International conference on machine learning*, pages 647–655. PMLR, 2014.
- Masahiro Kato, Takeshi Teshima, and Junya Honda. Learning from positive and unlabeled data with a selection bias. In *International Conference on Learning Representations*, 2018.
- Yu-Guan Hsieh, Gang Niu, and Masashi Sugiyama. Classification from positive, unlabeled and biased negative data. In *International Conference on Machine Learning*, pages 2820–2829. PMLR, 2019.
- Marthinus C Du Plessis, Gang Niu, and Masashi Sugiyama. Analysis of learning from positive and unlabeled data. *Advances in neural information processing systems*, 27:703–711, 2014.
- Jean Feydy, Thibault Séjourné, François-Xavier Vialard, Shun-ichi Amari, Alain Trounev, and Gabriel Peyré. Interpolating between optimal transport and mmd using sinkhorn divergences. In *The 22nd International Conference on Artificial Intelligence and Statistics*, pages 2681–2690, 2019b.

- Matthias Liero, Alexander Mielke, and Giuseppe Savaré. Optimal transport in competition with reaction: The hellinger–kantorovich distance and geodesic curves. *SIAM Journal on Mathematical Analysis*, 48(4):2869–2911, 2016.
- Lenaïc Chizat, Gabriel Peyré, Bernhard Schmitzer, and François-Xavier Vialard. An interpolating distance between optimal transport and fisher–rao metrics. *Foundations of Computational Mathematics*, 18(1):1–44, 2018c.
- Cedric Villani. *Topics in C. Transportation*. Graduate studies in Math. AMS, 2003.
- Rémi Flamary and Nicolas Courty. Pot python optimal transport library. *GitHub*: <https://github.com/rflamary/POT>, 2017.
- Christian Berg, Jens Peter Reus Christensen, and Paul Ressel. *Harmonic analysis on semigroups: theory of positive definite and related functions*, volume 100. Springer, 1984.

A Background on unbalanced optimal transport

Following Liero et al. [2015], this section reviews and generalizes the homogeneous and conic formulations of unbalanced optimal transport. These three formulations are equal in the convex setting of UOT. Our relaxed divergence UGW and conic distance CGW defined in Section 2 build upon those constructions but are not anymore equal due to the non-convexity of GW problems.

A.1 Homogeneous formulation

To ease the description of the homogeneous formulation, we develop and refactor the Csiszàr divergence terms of (1) in a form analog to Lemma 1. It reads

$$\text{UW}(\mu, \nu)^q = \inf_{\pi \in \mathcal{M}(X^2)} \int L_{\lambda(d(x,y))}(f(x), g(y)) d\pi(x, y) + \psi'_{\infty}(|\mu^{\perp}| + |\nu^{\perp}|), \quad (8)$$

where $L_c(r, s) \triangleq c + r\varphi(1/r) + s\varphi(1/s)$, $|\mu^{\perp}| \triangleq \mu^{\perp}(X)$ and $(f \triangleq \frac{d\mu}{d\pi_1}, g \triangleq \frac{d\nu}{d\pi_2})$ are the densities of the Lebesgue decomposition of (μ, ν) with respect to (π_1, π_2) and

$$\mu = f\pi_1 + \mu^{\perp} \quad \text{and} \quad \nu = g\pi_2 + \nu^{\perp}. \quad (9)$$

Such form is helpful to explicit the terms of pure mass creation/destruction ($|\mu^{\perp}| + |\nu^{\perp}|$) and reinterpret the integral under π as a transport term with a new cost $L_{\lambda(d)}$.

Then the authors of Liero et al. [2015] define the homogeneous formulations HUW as

$$\text{HUW}(\mu, \nu)^q \triangleq \inf_{\pi \in \mathcal{M}(X^2)} \int H_{\lambda(d(x,y))}(f(x), g(y)) d\pi(x, y) + \psi'_{\infty}(|\mu^{\perp}| + |\nu^{\perp}|), \quad (10)$$

where the 1-homogeneous function H_c is the perspective transform of L_c

$$H_c(r, s) \triangleq \inf_{\theta \geq 0} \theta(c + \psi(\frac{r}{\theta}) + \psi(\frac{s}{\theta})) = \inf_{\theta \geq 0} \theta L_c(\frac{r}{\theta}, \frac{s}{\theta}). \quad (11)$$

By definition one has $L_c \geq H_c$, though after optimization one has $\text{UW} = \text{HUW}$.

A.2 Cone sets, cone distances and explicit settings

The conic formulation detailed in Section A.3 is obtained by performing the optimal transport on the cone set $\mathfrak{C}[X] \triangleq X \times \mathbb{R}_+ / (X \times \{0\})$, where the extra coordinate accounts for the mass of the particle. Coordinates of the form $(x, 0)$ are merged into a single point called the apex of the cone, noted \mathfrak{o}_X . In the sequel, points of $X \times \mathbb{R}_+$ are noted (x, r) and those of $\mathfrak{C}[X]$ are noted $[x, r]$ to emphasize the quotient operation at the apex.

For a pair $(p, q) \in \mathbb{R}_+$, we define for any $[x, r], [y, s] \in \mathfrak{C}[X]^2$

$$\mathcal{D}_{\mathfrak{C}[X]}([x, r], [y, s])^q \triangleq H_{\lambda(d(x,y))}(r^p, s^p). \quad (12)$$

In general $\mathcal{D}_{\mathfrak{C}[X]}$ is not a distance, but it is always definite as proved by the following result described in De Ponti [2019].

Proposition 5. *Assume that d is definite, $\lambda^{-1}(\{0\}) = \{0\}$ and $\varphi^{-1}(\{0\}) = \{1\}$. Assume also that for any (r, s) , there always exists θ^* such that $H_c(r, s) = \theta^* L_c(\frac{r}{\theta^*}, \frac{s}{\theta^*})$. Then $\mathcal{D}_{\mathfrak{C}[X]}$ is definite on $\mathfrak{C}[X]$, i.e. $\mathcal{D}_{\mathfrak{C}[X]}([x, r], [y, s]) = 0$ if and only if $(r = s = 0)$ or $(r = s \text{ and } x = y)$.*

Proof. Assume $\mathcal{D}_{\mathfrak{C}[X]}([x, r], [y, s]) = 0$, and write θ^* such that

$$\mathcal{D}_{\mathfrak{C}[X]}([x, r], [y, s])^q = \theta^* L_c(\frac{r^p}{\theta^*}, \frac{s^p}{\theta^*}) = \theta^* \lambda(d(x, y)) + r^p \varphi(\frac{\theta^*}{r^p}) + s^p \varphi(\frac{\theta^*}{s^p}),$$

where the last line is given by the definition of reverse entropy. There are two cases. If $\theta^* > 0$, since all terms are positive, there are all equal to 0. By definiteness of d it yields $x = y$ and because $\varphi^{-1}(\{0\}) = \{1\}$ we have $r^p = s^p = \theta^*$ and $r = s$. If $\theta^* = 0$ then $\mathcal{D}_{\mathfrak{C}[X]}([x, r], [y, s])^q = \varphi(0)(r^p + s^p)$. The assumption $\varphi^{-1}(\{0\}) = \{1\}$ implies $\varphi(0) > 0$, thus necessarily $r = s = 0$. \square

The function H_c can be computed in closed form for a certain number of common entropies φ , and we refer to Liero et al. [2015, Section 5] for an overview. Of particular interest are those φ where $\mathcal{D}_{\mathfrak{C}[X]}$ is a distance, which necessitates a careful choice of λ, p and q . We now detail three particular settings where this is the case. In each setting we provide $(D_{\varphi}, \lambda, p, q)$ and its associated cone distance $\mathcal{D}_{\mathfrak{C}[X]}$.

Gaussian Hellinger distance It corresponds to

$$\begin{aligned} D_\varphi &= \text{KL}, \quad \lambda(t) = t^2 \quad \text{and} \quad q = p = 2, \\ \mathcal{D}_{\mathfrak{C}[X]}([x, r], [y, s])^2 &= r^2 + s^2 - 2rs e^{-d(x,y)/2}, \end{aligned}$$

in which case it is proved in Liero et al. [2015] that $\mathcal{D}_{\mathfrak{C}[X]}$ is a cone distance.

Hellinger-Kantorovich / Wasserstein-Fisher-Rao distance It reads

$$\begin{aligned} D_\varphi &= \text{KL}, \quad \lambda(t) = -\log \cos^2(t \wedge \frac{\pi}{2}) \quad \text{and} \quad q = p = 2, \\ \mathcal{D}_{\mathfrak{C}[X]}([x, r], [y, s])^2 &= r^2 + s^2 - 2rs \cos(\frac{\pi}{2} \wedge d(x, y)), \end{aligned}$$

in which case it is proved in Burago et al. [2001] that $\mathcal{D}_{\mathfrak{C}[X]}$ is a cone distance.

The weight $\lambda(t) = -\log \cos^2(t \wedge \frac{\pi}{2})$, which might seem more peculiar, is in fact the penalty that makes unbalanced OT a length space induced by the Gaussian-Hellinger distance (if the ground metric d is itself geodesic), as proved in Liero et al. [2016], Chizat et al. [2018c]. This weight introduces a cut-off, because $\lambda(d(x, y)) = +\infty$ if $d(x, y) > \pi/2$. There is no transport between points too far from each other. The choice of $\pi/2$ is arbitrary, and can be modified by scaling $\lambda \mapsto \lambda(\cdot/s)$ for some cutoff s .

Partial optimal transport It corresponds to

$$\begin{aligned} D_\varphi &= \text{TV}, \quad \lambda(t) = t^q \quad \text{and} \quad q \geq 1 \quad \text{and} \quad p = 1, \\ \mathcal{D}_{\mathfrak{C}[X]}([x, r], [y, s])^q &= r + s - (r \wedge s)(2 - d(x, y)^q)_+, \end{aligned}$$

in which case it is proved in Chizat et al. [2018a] that $\mathcal{D}_{\mathfrak{C}[X]}$ is a cone distance. The case $D_\varphi = \text{TV}$ is equivalent to partial unbalanced OT, which produces discontinuities (because of the non-smoothness of the divergence) between regions of the supports which are being transported and regions where mass is being destroyed/created. Note that Liero et al. [2015] do not mention that this $\mathcal{D}_{\mathfrak{C}[X]}$ defines a distance, so this result is new to the best of our knowledge, although it can be proved without a conic lifting that partial OT defines a distance as explained in Chizat et al. [2018a].

A.3 Conic formulation of UW

The last formulation reinterprets UW as an OT problem on the cone, with the addition of two linear constraints. Informally speaking, H_c becomes $\mathcal{D}_{\mathfrak{C}[X]}$, the term $(|\mu^\perp| + |\nu^\perp|)$ is taken into account by the constraints (14) below, and the variables (f, g) are replaced by (r^p, s^p) . It reads

$$\text{CUW}(\mu, \nu)^q \triangleq \inf_{\alpha \in \mathcal{U}_p(\mu, \nu)} \int \mathcal{D}_{\mathfrak{C}[X]}([x, r], [y, s])^q d\alpha([x, r], [y, s]), \quad (13)$$

where the constraint set $\mathcal{U}_p(\mu, \nu)$ is defined as

$$\mathcal{U}_p(\mu, \nu) \triangleq \left\{ \alpha \in \mathcal{M}_+(\mathfrak{C}[X]^2) : \int_{\mathbb{R}_+} r^p d\alpha_1(\cdot, r) = \mu, \int_{\mathbb{R}_+} s^p d\alpha_2(\cdot, s) = \nu \right\}. \quad (14)$$

Thus CUW consists in minimizing the Wasserstein distance $W_{\mathcal{D}_{\mathfrak{C}[X]}}(\alpha_1, \alpha_2)$ on the cone $(\mathfrak{C}[X], \mathcal{D}_{\mathfrak{C}[X]})$. The additional constraints on (α_1, α_2) mean that the lift of the mass on the cone must be consistent with the total mass of (μ, ν) . When $\mathcal{D}_{\mathfrak{C}[X]}$ is a distance, CUW inherits the metric properties of $W_{\mathcal{D}_{\mathfrak{C}[X]}}$. Our theoretical results rely on an analog construction for GW.

The following proposition states the equality of the three formulations and recapitulates its main properties. The proofs are detailed in Liero et al. [2015].

Proposition 6 (From Liero et al. [2015]). *One has $\text{UW} = \text{HUW} = \text{CUW}$, which are symmetric, positive and definite. Furthermore, if (X, d_X) and $(\mathfrak{C}[X], \mathcal{D}_{\mathfrak{C}[X]})$ are metric spaces with X separable, then $\mathcal{M}_+(X)$ endowed with CUW is a metric space.*

Proof. The equality $\text{UW} = \text{HUW}$ is given by Liero et al. [2015, Theorem 5.8], while the equality $\text{HUW} = \text{CUW}$ holds thanks to Liero et al. [2015, Theorem 6.7 and Remark 7.5], where the latter theorem can be straightforwardly generalized to any cone distance built as in Section 2.2.1. Since

$\mathcal{D}_{\mathfrak{C}[X]}$ is symmetric, positive and definite (see Proposition 3), then so is CUW. Furthermore, if $\mathcal{D}_{\mathfrak{C}[X]}$ satisfies the triangle inequality, separability of X allows to apply the gluing lemma [Liero et al., 2015, Corollary 7.14] which generalizes to any exponent p defining $\mathcal{U}_p(\mu, \nu)$ and any cone distance $\mathcal{D}_{\mathfrak{C}[X]}$. \square

B UGW formulation and definiteness

We present in this section the proofs of the properties of our divergence UGW. We refer to Section 2 for the definition of the UGW formulation and its related concepts. For conciseness we write $\Gamma(x, x', y, y') = |d_X(x, x') - d_Y(y, y')|$.

We first start with the existence of minimizers stated in Proposition 1. It illustrates in some sense that our divergence is well-defined.

Proposition 7 (Existence of minimizers). *Assume $(\mathcal{X}, \mathcal{Y})$ to be compact mm-spaces and that we either have*

1. φ superlinear, i.e $\varphi'_\infty = \infty$
2. λ has compact sublevel sets in \mathbb{R}_+ and $2\varphi'_\infty + \inf \lambda > 0$

Then there exists $\pi \in \mathcal{M}_+(X \times Y)$ such that $\text{UGW}(\mathcal{X}, \mathcal{Y}) = \mathcal{L}(\pi)$.

Proof. We adapt here from Liero et al. [2015, Theorem 3.3]. The functional is lower semi-continuous as a sum of l.s.c terms. Thus it suffices to have relative compactness of the set of minimizers. Under either one of the assumptions, coercivity of the functional holds thanks to Jensen's inequality

$$\begin{aligned} \mathcal{L}(\pi) &\geq m(\pi)^2 \inf \lambda(\Gamma) + m(\mu)^2 \varphi\left(\frac{m(\pi)^2}{m(\mu)^2}\right) + m(\nu)^2 \varphi\left(\frac{m(\pi)^2}{m(\nu)^2}\right) \\ &\geq m(\pi)^2 \left[\inf \lambda(\Gamma) + \frac{m(\mu)^2}{m(\pi)^2} \varphi\left(\frac{m(\pi)^2}{m(\mu)^2}\right) + \frac{m(\nu)^2}{m(\pi)^2} \varphi\left(\frac{m(\pi)^2}{m(\nu)^2}\right) \right]. \end{aligned}$$

As $m(\pi) \rightarrow +\infty$ the right hand side converges to $2\varphi'_\infty + \inf \lambda > 0$, which under either one of the assumptions yields $\mathcal{L}(\pi) \rightarrow +\infty$, hence the coercivity. Thus we can assume there exists some M such that $m(\pi) < M$. Since the spaces are assumed to be compact, the Banach-Alaoglu theorem holds and gives relative compactness in $\mathcal{M}_+(X \times Y)$.

Take any sequence of plans π_n that approaches $\text{UGW}(\mathcal{X}, \mathcal{Y}) = \inf \mathcal{L}(\pi)$. Compactness gives that a subsequence π_{n_k} weak* converges to some π^* . Because \mathcal{L} is l.s.c, we have $\mathcal{L}(\pi^*) \leq \inf \mathcal{L}(\pi)$, thus $\mathcal{L}(\pi^*) = \inf \mathcal{L}(\pi)$. The existence of such limit reaching the infimum gives the existence of a minimizer. \square

Note that this formulation is nonnegative and symmetric because the functional \mathcal{L} is also nonnegative and symmetric in its inputs $(\mathcal{X}, \mathcal{Y})$. This formulation allows straightforwardly to prove the definiteness of UGW.

Proposition 8 (Definiteness of UGW). *Assume that $\varphi^{-1}(\{0\}) = \{1\}$ and $\lambda^{-1}(\{0\}) = \{0\}$. The following assertions are equivalent:*

1. $\text{UGW}(\mathcal{X}, \mathcal{Y}) = 0$
2. $\exists \pi \in \mathcal{M}_+(X \times Y)$ whose marginals are (μ, ν) such that $d_X(x, x') = d_Y(y, y')$ for $\pi \otimes \pi$ -a.e. $(x, x', y, y') \in (X \times Y)^2$.
3. There exists a mm-space (Z, d_Z, η) with full support and Borel maps $\psi_X : Z \rightarrow X$ and $\psi_Y : Z \rightarrow Y$. such that $(\psi_X)_\# \eta = \mu$, $(\psi_Y)_\# \eta = \nu$ and $d_Z = (\psi_X)^\# d_X = (\psi_Y)^\# d_Y$
4. There exists a Borel measurable bijection between the measures' supports $\psi : \text{spt}(\mu) \rightarrow \text{spt}(\nu)$ with Borel measurable inverse such that $\psi_\# \mu = \nu$ and $d_Y = \psi^\# d_X$.

Proof. Recall that (2) \Leftrightarrow (3) \Leftrightarrow (4) from Sturm [2012, Lemma 1.10]. thus it remains to prove (1) \Leftrightarrow (2).

If there is such coupling plan π between (μ, ν) then one has $\pi \otimes \pi$ -a.e. that $\Gamma = 0$, and all φ -divergences are zero as well, yielding a distance of zero a.e.

Assume now that $\text{UGW}(\mathcal{X}, \mathcal{Y}) = 0$, and write π an optimal plan. All terms of \mathcal{L} are positive, thus under our assumptions we have $\Gamma = 0$, $\pi_1 \otimes \pi_1 = \mu \otimes \mu$ and $\pi_2 \otimes \pi_2 = \nu \otimes \nu$. Thus we get that π has marginals (μ, ν) and that $d_X(x, x') = d_Y(y, y')$ $\pi \otimes \pi$ -a.e. \square

We end with a result on the reformulation of UGW which is the first step to connect it with the conic formulation CGW. It is the same proof as in the main body.

Lemma 2. *Defining $L_c(r, s) \triangleq c + r\varphi(1/r) + s\varphi(1/s)$, and writing $(f \triangleq \frac{d\mu}{d\pi_1}, g \triangleq \frac{d\nu}{d\pi_2})$ the Lebesgue densities of (μ, ν) w.r.t. (π_1, π_2) such that $\mu = f\pi_1 + \mu^\perp$ and $\nu = g\pi_2 + \nu^\perp$, one has*

$$\mathcal{L}(\pi) = \int_{X^2 \times Y^2} L_{\lambda(\Gamma)}(f \otimes f, g \otimes g) d\pi d\pi + \varphi(0)(|(\mu \otimes \mu)^\perp| + |(\nu \otimes \nu)^\perp|).$$

Proof. Using Equation (24), one has

$$\begin{aligned} \mathcal{L}(\pi) &= \int_{X^2 \times Y^2} \lambda(\Gamma) d\pi d\pi + \mathbf{D}_\varphi^\otimes(\pi_1|\mu) + \mathbf{D}_\varphi^\otimes(\pi_2|\nu) \\ &= \int_{X^2 \times Y^2} \lambda(\Gamma) d\pi d\pi + \mathbf{D}_\psi^\otimes(\mu|\pi_1) + \mathbf{D}_\psi^\otimes(\nu|\pi_2) \\ &= \int_{X^2 \times Y^2} \lambda(\Gamma) d\pi d\pi + \int_{X^2} \psi(f \otimes f) d\pi_1 d\pi_1 + \int_{Y^2} \psi(g \otimes g) d\pi_2 d\pi_2 \\ &\quad + \varphi(0)(|(\mu \otimes \mu)^\perp| + |(\nu \otimes \nu)^\perp|) \\ &= \int_{X^2 \times Y^2} L_{\lambda(\Gamma)}(f \otimes f, g \otimes g) d\pi d\pi + \varphi(0)(|(\mu \otimes \mu)^\perp| + |(\nu \otimes \nu)^\perp|). \end{aligned}$$

□

C Conic formulation and metric properties

We present in this section the proofs of the properties mentioned in Section 2. We refer to Section 2 and Appendix A for the definition of the conic formulation and its related concepts.

In this section we frequently use the notion of marginal for neasures. For any sets E, F , we write $\mathfrak{P}^{(E)} : E \times F \rightarrow E$ the **canonical projection** such that for any $(x, y) \in E \times F$, $\mathfrak{P}^{(E)}(x, y) = x$. Consider two complete separable mm-spaces $\mathcal{X} = (X, d_X, \mu)$ and $\mathcal{Y} = (Y, d_Y, \nu)$. Write $\pi \in \mathcal{M}_+(X \times Y)$ a coupling plan, and define its marginals by $\pi_1 = \mathfrak{P}_\#^{(X)}\pi$ and $\pi_2 = \mathfrak{P}_\#^{(Y)}\pi$. The definition of the marginals can also be seen by the use of test functions. In the case of π_1 it reads for any test function ξ

$$\int \xi(x) d\pi_1(x) = \int \xi(x) d\pi(x, y).$$

C.1 Preliminary results

We present in this section concepts and properties which are necessary for the proof of Theorem 1. We introduce a dilation operator whose role is to rescale the radial coordinate of a measure with a given scaling.

Definition 2 (dilations). *Consider $v([x, r], [y, s])$ a Borel measurable scaling function depending on $[x, r], [y, s] \in \mathfrak{C}[X] \times \mathfrak{C}[Y]$. Take a plan $\alpha \in \mathcal{M}_+(\mathfrak{C}[X] \times \mathfrak{C}[Y])$. We define the dilation $\text{Dil}_v : \alpha \mapsto (h_v)_\#(v^p\alpha)$ where*

$$h_v([x, r], [y, s]) \triangleq ([x, r/w], [y, s/w]),$$

where $w = v([x, r], [y, s])$. It reads for any test function ξ

$$\int \xi([x, r], [y, s]) d\text{Dil}_v(\alpha) = \int \xi([x, r/w], [y, s/w]) w^p d\alpha.$$

The importance of dilations is given by the following lemma.

Lemma 3 (Invariance to dilation). *The problem CGW is invariant to dilations, i.e. for any $\alpha \in \mathcal{U}_p(\mu, \nu)$, we have $\text{Dil}_v(\alpha) \in \mathcal{U}_p(\mu, \nu)$ and $\mathcal{H}(\alpha) = \mathcal{H}(\text{Dil}_v(\alpha))$.*

Proof. First we prove the stability of $\mathcal{U}_p(\mu, \nu)$ under dilations. Take $\alpha \in \mathcal{U}_p(\mu, \nu)$. For any test function ξ defined on X we have

$$\int \xi(x) r^p d\text{Dil}_v(\alpha) = \int \xi(x) \left(\frac{r}{v}\right)^p \cdot v^p d(\alpha) = \int \xi(x) r^p d\alpha = \int \xi(x) d\mu(x).$$

Similarly we get $\mathfrak{P}_\#^{(Y)}(s^q \text{Dil}_v(\alpha)) = \nu$, thus $\text{Dil}_v(\alpha) \in \mathcal{U}_p(\mu, \nu)$.

It remains to prove the invariance of the functional. Recall that \mathcal{D}^q is p -homogeneous. It yields

$$\begin{aligned} \mathcal{H}(\text{Dil}_v(\alpha)) &= \int \mathcal{D}([d_X(x, x'), rr'], [d_Y(y, y'), ss'])^q d\text{Dil}_v(\alpha) d\text{Dil}_v(\alpha) \\ &= \int \mathcal{D}([d_X(x, x'), \frac{r}{v} \cdot \frac{r'}{v}], [d_Y(y, y'), \frac{s}{v} \cdot \frac{s'}{v}])^q v^p \cdot v^p d\alpha d\alpha \\ &= \int \frac{1}{v^{2p}} \mathcal{D}([d_X(x, x'), rr'], [d_Y(y, y'), ss'])^q v^{2p} d\alpha d\alpha \\ &= \int \mathcal{D}([d_X(x, x'), rr'], [d_Y(y, y'), ss'])^q d\alpha d\alpha \\ &= \mathcal{H}(\alpha) \end{aligned}$$

Both the functional and the constraint set are invariant, thus the whole CGW problem is invariant to dilations. \square

The above lemma allows to normalize the plan such that one of its marginal is fixed to some value. Fixing a marginal allows to generalize the gluing lemma which is a key ingredient of the triangle inequality in optimal transport.

Lemma 4 (Normalization lemma). *Assume there exists $\alpha \in \mathcal{U}_p(\mu, \nu)$ such that $\text{CGW}(\mathcal{X}, \mathcal{Y}) = \mathcal{H}(\alpha)$. Then there exists $\tilde{\alpha}$ such that $\tilde{\alpha} \in \mathcal{U}_p(\mu, \nu)$ and $\text{CGW}(\mathcal{X}, \mathcal{Y}) = \mathcal{H}(\tilde{\alpha})$ and whose marginal on $\mathfrak{C}[Y]$ is $\nu_{\mathfrak{C}[Y]} = \mathfrak{P}^{(\mathfrak{C}[Y])\#} \tilde{\alpha} = \delta_{\mathfrak{o}_Y} + \mathfrak{p}_\#(\nu \otimes \delta_1)$, where \mathfrak{p} is the canonical injection from $Y \times \mathbb{R}_+$ to $\mathfrak{C}[Y]$.*

Proof. The proof is exactly the same as Liero et al. [2015, Lemma 7.10] and is included for completeness. Take an optimal plan α . Because the functional and the constraints are homogeneous in (r, s) , the plan $\hat{\alpha} = \alpha + \delta_{\mathfrak{o}_X} \otimes \delta_{\mathfrak{o}_Y}$ verifies $\hat{\alpha} \in \mathcal{U}_p(\mu, \nu)$ and $\mathcal{H}(\hat{\alpha}) = \mathcal{H}(\alpha)$. Indeed, because of this homogeneity the contribution $\delta_{\mathfrak{o}_X} \otimes \delta_{\mathfrak{o}_Y}$ has $(r, s) = (0, 0)$ which has thus no impact.

Considering $\hat{\alpha}$ instead of α allows to assume without loss of generality that the transport plan charges the apex, i.e. setting

$$S = \{[x, r], [y, s] \in \mathfrak{C}[X] \times \mathfrak{C}[Y], [y, s] = \mathfrak{o}_Y\}, \quad (15)$$

one has $\omega_Y \triangleq \hat{\alpha}(S) \geq 1$. Then we can define the following scaling

$$v([x, r], [y, s]) = \begin{cases} s & \text{if } s > 0 \\ \omega_Y^{-1/q} & \text{otherwise.} \end{cases} \quad (16)$$

We prove now that $\text{Dil}_v(\hat{\alpha})$ has the desired marginal on $\mathfrak{C}(Y)$ by considering test functions $\xi([y, s])$. We separate the integral into two parts with the set S , and write $\hat{\alpha} = \hat{\alpha}|_S + \hat{\alpha}|_{S^c}$ their restrictions to S and S^c respectively. It reads

$$\begin{aligned} \int \xi([y, s]) d\text{Dil}_v(\hat{\alpha}) &= \int \xi([y, s/v]) v^p d\hat{\alpha} \\ &= \int \xi([y, s/v]) v^p d\hat{\alpha}|_S + \int \xi([y, s/v]) v^p d\hat{\alpha}|_{S^c} \\ &= \int \xi(\mathfrak{o}_Y) \omega_Y^{-1} d\hat{\alpha}|_S + \int \xi([y, s/s]) s^p d\hat{\alpha}|_{S^c} \\ &= \xi(\mathfrak{o}_Y) \cdot \omega_Y \cdot \omega_Y^{-1} + \int \xi([y, 1]) s^p d\hat{\alpha} \\ &= \xi(\mathfrak{o}_Y) + \int \xi(\mathfrak{p}(y, s)) d(\nu(y) \otimes \delta_1(s)) \\ &= \int \xi([y, s]) d(\delta_{\mathfrak{o}_Y} + \mathfrak{p}_\#(\nu \otimes \delta_1)), \end{aligned}$$

which is the formula of the desired marginal on $\mathfrak{C}[Y]$. Since $\hat{\alpha} \in \mathcal{U}_p(\mu, \nu)$, its dilation is also in $\mathcal{U}_p(\mu, \nu)$, and $\mathcal{H}(\alpha) = \mathcal{H}(\hat{\alpha}) = \mathcal{H}(\text{Dil}_v(\hat{\alpha}))$. \square

C.1.1 Proof of Theorem 1

Non-negativity and *symmetry* hold since \mathcal{H} is a sum of non-negative symmetric terms. To prove *Definiteness*, assume $\text{CGW}(\mathcal{X}, \mathcal{Y}) = 0$, and write α an optimal plan. We have $\alpha \otimes \alpha$ -a.e. that $d_X(x, x') = d_Y(y, y')$ and $rr' = ss'$ because \mathcal{D} is definite (see Proposition 3). Thanks to the completeness of $(\mathcal{X}, \mathcal{Y})$ and a result from Sturm [2012, Lemma 1.10], such property implies the existence of a Borel isometric bijection with Borel inverse between the supports of the measures $\psi : \text{Supp}(\mu) \rightarrow \text{Supp}(\nu)$, where Supp denotes the support. The bijection ψ verifies $d_X(x, x') = d_Y(\psi(x), \psi(x'))$. To prove $\mathcal{X} \sim \mathcal{Y}$ it remains to prove $\psi_{\#}\mu = \nu$. Due to the density of continuous functions of the form $\xi(x)\xi(x')$, the constraints of $\mathcal{U}_p(\mu, \nu)$ are equivalent to

$$\int_{\mathbb{R}_+} (rr')^p d\alpha_1(\cdot, r) d\alpha_1(\cdot, r') = \mu \otimes \mu, \quad \int_{\mathbb{R}_+} (ss')^p d\alpha_2(\cdot, s) d\alpha_2(\cdot, s') = \nu \otimes \nu.$$

Take a continuous test function ξ defined on $\text{Supp}(\nu)^2$. Writing $y = \psi(x)$ and $y' = \psi(x')$, one has

$$\begin{aligned} \int \xi(y, y') d\nu d\nu &= \int \xi(y, y') (ss')^p d\alpha d\alpha \\ &= \int \xi(\psi(x), \psi(x')) (ss')^p d\alpha d\alpha \\ &= \int \xi(\psi(x), \psi(x')) (rr')^p d\alpha d\alpha \\ &= \int \xi(\psi(x), \psi(x')) d\mu d\mu \\ &= \int \tilde{\xi}(x, x') d\psi_{\#}\mu d\psi_{\#}\mu. \end{aligned}$$

Since ψ is a bijection, there is a bijection between continuous functions ξ of $\text{Supp}(\nu)^2$ and functions $\tilde{\xi}$ of $\text{Supp}(\mu)^2$. Thus we obtain $\nu = \psi_{\#}\mu$ and we have $\mathcal{X} \sim \mathcal{Y}$.

It remains to prove the *triangle inequality*. Assume now that \mathcal{D} satisfies it. Given three mm-spaces $(\mathcal{X}, \mathcal{Y}, \mathcal{Z})$ respectively equipped with measures (μ, ν, η) , consider α, β which are optimal plans for $\text{CGW}(\mathcal{X}, \mathcal{Y})$ and $\text{CGW}(\mathcal{Y}, \mathcal{Z})$. Using Lemma 4 to both α and β , we can consider measures $(\bar{\alpha}, \bar{\beta})$ which are also optimal and have a common marginal $\bar{\nu}$ on $\mathfrak{C}[Y]$. Thanks to this common marginal and the separability of (X, Y, Z) , the standard gluing lemma [Villani, 2003, Lemma 7.6] applies and yields a glued plan $\gamma \in \mathcal{M}_+(\mathfrak{C}[X] \times \mathfrak{C}[Y] \times \mathfrak{C}[Z])$ whose respective marginals on $\mathfrak{C}[X] \times \mathfrak{C}[Y]$ and $\mathfrak{C}[Y] \times \mathfrak{C}[Z]$ are $(\bar{\alpha}, \bar{\beta})$. Furthermore, the marginal $\bar{\gamma}$ of γ on $\mathfrak{C}[X] \times \mathfrak{C}[Z]$ is in $\mathcal{U}_p(\mu, \eta)$. Indeed, $(\bar{\gamma}, \bar{\alpha})$ have the same marginal on $\mathfrak{C}[X]$ and same for $(\bar{\gamma}, \bar{\beta})$ on $\mathfrak{C}[Z]$, hence this property. Write

$d_X = d_X(x, x')$ for sake of conciseness (and similarly for Y, Z). The calculation reads

$$\text{CGW}(\mathcal{X}, \mathcal{Z})^{\frac{1}{q}} \tag{17}$$

$$\leq \left(\int \mathcal{D}([d_X, rr'], [d_Z, tt'])^q d\bar{\gamma}([x, r], [z, t]) d\bar{\gamma}([x', r'], [z', t']) \right)^{\frac{1}{q}} \tag{18}$$

$$\leq \left(\int \mathcal{D}([d_X, rr'], [d_Z, tt'])^q d\gamma([x, r], [y, s], [z, t]) d\gamma([x', r'], [y', s'], [z', t']) \right)^{\frac{1}{q}} \tag{19}$$

$$\leq \left(\int (\mathcal{D}([d_X, rr'], [d_Y, ss']) + \mathcal{D}([d_Y, ss'], [d_Z, tt']))^q d\gamma d\gamma \right)^{\frac{1}{q}} \tag{20}$$

$$\leq \left(\int \mathcal{D}([d_X, rr'], [d_Y, ss'])^q d\gamma d\gamma \right)^{\frac{1}{q}} + \left(\int \mathcal{D}([d_Y, ss'], [d_Z, tt'])^q d\gamma d\gamma \right)^{\frac{1}{q}} \tag{21}$$

$$\leq \left(\int \mathcal{D}([d_X, rr'], [d_Y, ss'])^q d\bar{\alpha}([x, r], [y, s]) d\bar{\alpha}([x', r'], [y', s']) \right)^{\frac{1}{q}} \\ + \left(\int \mathcal{D}([d_Y, ss'], [d_Z, tt'])^q d\bar{\beta}([y, s], [z, t]) d\bar{\beta}([y', s'], [z', t']) \right)^{\frac{1}{q}} \tag{22}$$

$$\leq \text{CGW}(\mathcal{X}, \mathcal{Y})^{\frac{1}{q}} + \text{CGW}(\mathcal{Y}, \mathcal{Z})^{\frac{1}{q}}. \tag{23}$$

Since $\bar{\gamma} \in \mathcal{U}_p(\mu, \eta)$, it is thus suboptimal, which yields Equation (18). Because $\bar{\gamma}$ is the marginal of γ we get Equation (19). Equations (20) and (21) are respectively obtained by the triangle and Minkowski inequalities, which hold because \mathcal{D} which is a distance. Equation (22) is the marginalization of γ , and Equation (23) is given by the optimality of $(\bar{\alpha}, \bar{\beta})$, which ends the proof of the triangle inequality.

C.1.2 Proof of the inequality between UGW and CGW

The proof consists in considering an optimal plan π for UGW, building a lift α of this plan into the cone such that $\mathcal{L}(\pi) \geq \mathcal{H}(\alpha)$, and prove that α is admissible for the program CGW, thus suboptimal.

Using Equation (9), we have

$$\begin{aligned} \mu \otimes \mu &= (f \otimes f)\pi_1 \otimes \pi_1 + (\mu \otimes \mu)^\perp, \\ (\mu \otimes \mu)^\perp &= \mu^\perp \otimes (f\pi_1) + (f\pi_1) \otimes \mu^\perp + \mu^\perp \otimes \mu^\perp, \\ \nu \otimes \nu &= (g \otimes g)\pi_2 \otimes \pi_2 + (\nu \otimes \nu)^\perp, \\ (\nu \otimes \nu)^\perp &= \nu^\perp \otimes (g\pi_2) + (g\pi_2) \otimes \nu^\perp + \nu^\perp \otimes \nu^\perp. \end{aligned} \tag{24}$$

Recall that the canonic injection \mathbf{p} reads $\mathbf{p}(x, r) = [x, r]$. Based on the above Lebesgue decomposition, we define the conic plan

$$\alpha = (\mathbf{p}(x, f(x)^{\frac{1}{p}}), \mathbf{p}(y, g(y)^{\frac{1}{p}}))_{\#} \pi(x, y) + \delta_{\mathfrak{o}_X} \otimes \mathbf{p}_{\#}[\nu^\perp \otimes \delta_1] + \mathbf{p}_{\#}[\mu^\perp \otimes \delta_1] \otimes \delta_{\mathfrak{o}_Y}. \tag{25}$$

We have that $\alpha \in \mathcal{U}_p(\mu, \nu)$. Indeed for the first marginal (and similarly for the second) we have for any test function $\xi(x)$

$$\begin{aligned} \int \xi(x)(r)^p d\alpha &= \int \xi(x)f(x)d\pi_1(x) + 0 + \int \xi(x)(1)^p d\mu^\perp(x) \\ &= \int \xi(x)d(f(x)\pi_1 + \mu^\perp) \\ &= \int \xi(x)d\mu(x). \end{aligned}$$

We define $\theta^* = \theta_c^*(r, s)$ the parameter which verifies $H_c(r, s) = \theta^* L_c(r/\theta^*, s/\theta^*)$. We restrict $\alpha \otimes \alpha$ to the set $S = \{\theta_{\chi(\Gamma)}^*((rr')^p, (ss')^p) > 0\}$. By construction, $\theta_c^*(r, s)$ is 1-homogeneous in (r, s) . Thus on S we necessarily have $r, r', s, s' > 0$. It yields

$$\alpha \otimes \alpha|_S = (\mathbf{p}(x, f(x)^{\frac{1}{p}}), \mathbf{p}(y, g(y)^{\frac{1}{p}}), \mathbf{p}(x', f(x')^{\frac{1}{p}}), \mathbf{p}(y', g(y')^{\frac{1}{p}}))_{\#} (\pi \otimes \pi).$$

Concerning the orthogonal part of the decomposition, note that whenever $\theta^* = 0$, due to the definition of H the cone distance reads

$$\mathcal{D}([x, r], [y, s])^q = \varphi(0)(r^p + s^p). \quad (26)$$

It geometrically means that the shortest path between $[x, r]$ and $[y, s]$ must pass via the apex, which corresponds to a pure mass creation/destruction regime.

Furthermore we have that

$$\begin{aligned} |(\mu \otimes \mu)^\perp| &= \int (r \cdot r')^p d(\alpha \otimes \alpha)|_{S^c}, \\ |(\nu \otimes \nu)^\perp| &= \int (s \cdot s')^p d(\alpha \otimes \alpha)|_{S^c}. \end{aligned}$$

Indeed, thanks to Equation (25) we have for the first marginal that

$$\begin{aligned} |(\mu \otimes \mu)^\perp| &= (\mu^\perp \otimes (f\pi_1) + (f\pi_1) \otimes \mu^\perp + \mu^\perp \otimes \mu^\perp)(X^2) \\ &= \int (rr')^p d\mathbf{p}_\#[\mu^\perp \otimes \delta_1] d\mathbf{p}(x', f(x')^{\frac{1}{p}})_\# \pi_1(x') \\ &\quad + \int (rr')^p d\mathbf{p}(x, f(x)^{\frac{1}{p}})_\# \pi_1(x) d\mathbf{p}_\#[\mu^\perp \otimes \delta_1] \\ &\quad + \int (rr')^p d\mathbf{p}_\#[\mu^\perp \otimes \delta_1] d\mathbf{p}_\#[\mu^\perp \otimes \delta_1] \\ &= \int (rr')^p d(\alpha \otimes \alpha)|_{S^c}. \end{aligned}$$

Note that the last equality holds because each term of $\alpha \otimes \alpha$ involving a measure δ_{\circ_X} cancels out when integrated against $(rr')^p$.

Eventually the computation gives (thanks to Lemma 1)

$$\begin{aligned} \mathcal{L}(\pi) &= \int_{X^2 \times Y^2} L_{\lambda(\Gamma)}(f \otimes f, g \otimes g) d\pi d\pi + \varphi(0)(|(\mu \otimes \mu)^\perp| + |(\nu \otimes \nu)^\perp|) \\ &\geq \int H_{\lambda(\Gamma)}(f \otimes f, g \otimes g) d\pi d\pi + \varphi(0)(|(\mu \otimes \mu)^\perp| + |(\nu \otimes \nu)^\perp|) \\ &\geq \int \mathcal{D}([d_X(x, x'), (f \otimes f)^{\frac{1}{p}}], [d_Y(y, y'), (g \otimes g)^{\frac{1}{p}}])^q d\pi d\pi \\ &\quad + \int \varphi(0)(rr')^p d(\alpha \otimes \alpha)|_{S^c} + \int \varphi(0)(ss')^p d(\alpha \otimes \alpha)|_{S^c} \\ &\geq \int \mathcal{D}([d_X(x, x'), rr'], [d_Y(y, y'), ss'])^q d(\alpha \otimes \alpha)|_S \\ &\quad + \int \varphi(0)((rr')^p + (ss')^p) d(\alpha \otimes \alpha)|_{S^c} \\ &\geq \int \mathcal{D}([d_X(x, x'), rr'], [d_Y(y, y'), ss'])^q d\alpha d\alpha \\ &\geq \mathcal{H}(\alpha). \end{aligned}$$

Thus we have $\text{UGW}(\mathcal{X}, \mathcal{Y}) = \mathcal{L}(\pi) \geq \mathcal{H}(\alpha) \geq \text{CGW}(\mathcal{X}, \mathcal{Y})$.

D Optimization, algorithms and formulas

We present in this section the important results of Section 3. We start with Theorem 2 stating that for a wide range of quadratic programs, performing a bi-convex relaxation yields the same objective value as the original program. We prove its application in Theorem 3. We provide a decomposition property of KL^{\otimes} , followed by the proof of Proposition 4, and a description of the algorithm in a discrete setting, where computationally implementable formulas are provided.

D.1 Proof of Theorem 2

Proof. The function \mathcal{F} is the symmetrization of \mathcal{L} , so that $\mathcal{F}(\pi, \pi) = \mathcal{L}(\pi)$. By the hypothesis on \mathcal{L} , the minimum values of the functions (if it exists) are finite. The two following inequalities are obtained by optimality of (π_*, γ_*) ,

$$\begin{cases} \mathcal{F}(\pi_*, \gamma_*) \leq \mathcal{F}(\pi_*, \pi_*) \\ \mathcal{F}(\pi_*, \gamma_*) \leq \mathcal{F}(\gamma_*, \gamma_*) \end{cases} \quad (27)$$

Note that the hypotheses imply that $\mathcal{F}(\pi_*, \pi_*)$ and $\mathcal{F}(\gamma_*, \gamma_*)$ are both finite. Combining these two inequalities leads to $\mathcal{F}(\pi_*, \pi_*) + \mathcal{F}(\gamma_*, \gamma_*) - 2\mathcal{F}(\pi_*, \gamma_*) \geq 0$, which implies

$$\frac{1}{2} \langle \pi_* - \gamma_*, k(\pi_* - \gamma_*) \rangle \geq 0, \quad (28)$$

since the separable parts in \mathcal{F} cancel. Since k is negative, we also have the converse inequality, thus $\frac{1}{2} \langle \pi_* - \gamma_*, k(\pi_* - \gamma_*) \rangle = 0$. Therefore, we deduce when k is definite that $\pi_* = \gamma_*$.

We now treat the case when k is not definite. In this case, we only have $\frac{1}{2} \langle \pi_* - \gamma_*, k(\pi_* - \gamma_*) \rangle = 0$ which implies that $\pi_* - \gamma_* \in \text{Ker}(k)$ since k is non positive. The first inequality in (27) implies $f(\pi_*) \leq f(\gamma_*)$ and by symmetry $f(\pi_*) = f(\gamma_*)$ and as a conclusion $\mathcal{F}(\pi_*, \pi_*) = \mathcal{F}(\pi_*, \gamma_*) = \mathcal{F}(\gamma_*, \gamma_*)$.

The last case follows from the observation that on the segment $[\pi_*, \gamma_*] \subset C$, the quadratic part of \mathcal{F} is constant. Indeed one has for $t \in [0, 1]$, for $z = t(\pi_* - \gamma_*) + \gamma_*$ one has

$$\langle z, k(z) \rangle = t^2 \langle (\pi_* - \gamma_*), k(\pi_* - \gamma_*) \rangle + 2t \langle \gamma_*, k(\pi_* - \gamma_*) \rangle + \langle \gamma_*, k(\gamma_*) \rangle = \langle \gamma_*, k(\gamma_*) \rangle,$$

since $\pi_* - \gamma_* \in \text{Ker}(k)$. Thus minimizing \mathcal{F} on $[\pi_*, \gamma_*]$ is reduced to the minimization of f on this segment. By the above remark, $f(\pi_*) = f(\gamma_*)$ which implies $\pi_* = \gamma_*$ by strict convexity. \square

D.2 Properties of the quadratic KL divergence

We present in this section an additional property on the quadratic-KL divergence which allows to reduce the computational burden to evaluate it by involving the computation of a standard KL divergence.

Proposition 9. *For any measures $(\mu, \nu) \in \mathcal{M}_+(\mathcal{X})$, one has*

$$\begin{aligned} \text{KL}(\mu \otimes \nu | \alpha \otimes \beta) &= m(\nu) \text{KL}(\mu | \alpha) + m(\mu) \text{KL}(\nu | \beta) \\ &\quad + (m(\mu) - m(\alpha))(m(\nu) - m(\beta)). \end{aligned} \quad (29)$$

In particular,

$$\text{KL}(\mu \otimes \mu | \nu \otimes \nu) = 2m(\mu) \text{KL}(\mu | \nu) + (m(\mu) - m(\nu))^2. \quad (30)$$

Proof. Assuming $\text{KL}(\mu \otimes \nu | \alpha \otimes \beta)$ to be finite, one has $\mu = f\alpha$ and $\nu = g\beta$. It reads

$$\begin{aligned}
\text{KL}(\mu \otimes \nu | \alpha \otimes \beta) &= \int \log(f \otimes g) d\mu d\nu - m(\mu)m(\nu) + m(\alpha)m(\beta) \\
&= m(\nu) \int \log(f) d\mu + m(\mu) \int \log(g) d\nu \\
&\quad - m(\mu)m(\nu) + m(\alpha)m(\beta) \\
&= m(\nu) [\text{KL}(\mu | \alpha) + m(\mu) - m(\alpha)] \\
&\quad + m(\mu) [\text{KL}(\nu | \beta) + m(\nu) - m(\beta)] \\
&\quad - m(\mu)m(\nu) + m(\alpha)m(\beta) \\
&= m(\nu)\text{KL}(\mu | \alpha) + m(\mu)\text{KL}(\nu | \beta) \\
&\quad + m(\mu)m(\nu) - m(\nu)m(\alpha) - m(\mu)m(\beta) + m(\alpha)m(\beta) \\
&= m(\nu)\text{KL}(\mu | \alpha) + m(\mu)\text{KL}(\nu | \beta) \\
&\quad + (m(\mu) - m(\alpha))(m(\nu) - m(\beta)).
\end{aligned}$$

□

In the Balanced setting, with (μ, ν) probabilities, the regularization reads $\text{KL}^\otimes(\pi | \mu \otimes \nu) = 2\text{KL}(\pi | \mu \otimes \nu)$. Thus (up to a factor 2) we retrieve as a particular case the setting of Peyré et al. [2016].

D.3 Proof of Proposition 4

We now prove Proposition 4 which applies the above result.

Proposition 10. *For a fixed γ , the optimal $\pi \in \arg \min_{\pi} \mathcal{F}(\pi, \gamma) + \varepsilon \text{KL}(\pi \otimes \gamma | (\mu \otimes \nu)^{\otimes 2})$ is the solution of $\min_{\pi} \int c_{\gamma}^{\varepsilon}(x, y) d\pi(x, y) + \rho m(\gamma) \text{KL}(\pi_1 | \mu) + \rho m(\gamma) \text{KL}(\pi_2 | \nu) + \varepsilon m(\gamma) \text{KL}(\pi | \mu \otimes \nu)$, where $m(\gamma) \triangleq \gamma(X \times Y)$ is the total mass of γ , and where we define the cost and weight associated to γ as*

$$c_{\gamma}^{\varepsilon}(x, y) \triangleq \int \lambda(\Gamma(x, \cdot, y, \cdot)) d\gamma + \rho \int \log\left(\frac{d\gamma_1}{d\mu}\right) d\gamma_1 + \rho \int \log\left(\frac{d\gamma_2}{d\nu}\right) d\gamma_2 + \varepsilon \int \log\left(\frac{d\gamma}{d\mu d\nu}\right) d\gamma.$$

Proof. First note that $\mathcal{F}(\gamma, \pi) = \mathcal{F}(\pi, \gamma)$ so that minimizing with the first or the second argument gives the same solution. Setting γ to be fixed, the rest follows from the factorisation

$$\begin{aligned}
\text{KL}(\pi_1 \otimes \gamma_1 | \mu \otimes \mu) &= m(\gamma) \text{KL}(\pi_1 | \mu) + m(\pi) \text{KL}(\gamma_1 | \mu) + (m(\gamma) - m(\mu))(m(\pi) - m(\mu)) \\
&= m(\pi) \left[\text{KL}(\gamma_1 | \mu) + m(\gamma) - m(\mu) \right] + m(\gamma) \text{KL}(\pi_1 | \mu) - m(\gamma) m(\mu) \\
&= m(\pi) \int \log\left(\frac{d\gamma_1}{d\mu}\right) d\gamma_1 + m(\gamma) \text{KL}(\pi_1 | \mu) - m(\gamma) m(\mu) \\
&= \int \left(\int \log\left(\frac{d\gamma_1}{d\mu}\right) d\gamma_1 \right) d\pi + m(\gamma) \text{KL}(\pi_1 | \mu) - m(\gamma) m(\mu),
\end{aligned}$$

and also from $\text{KL}(\pi_1 | \mu) = \int \log\left(\frac{d\gamma_1}{d\mu}\right) d\gamma_1 - (m(\gamma) - m(\mu))$. Similar formulas hold for (π_2, γ_2) and (π, γ) . Summing all KL terms yields the expression for c_{γ}^{ε} . □

D.4 Discrete setting and formulas

In order to implement those algorithms, one consider discrete mm-spaces $X = (x_i)_{i=1}^n$ and $Y = (y_j)_{j=1}^m$, endowed with discrete measures $\mu = \sum_i \mu_i \delta_{x_i}$ and $\nu = \sum_j \nu_j \delta_{y_j}$, where $\mu_i, \nu_j \geq 0$. The distance matrices are $D_{i,i'}^X \triangleq d_X(x_i, x_{i'})$ and $D_{j,j'}^Y \triangleq d_X(y_j, y_{j'})$. Transport plans are thus also discrete $\pi = \sum_{i,j} \pi_{i,j} \delta_{(x_i, y_j)}$.

Algorithm 2 – UGW($\mathcal{X}, \mathcal{Y}, \rho, \varepsilon$) in discrete form

Input: mm-spaces $\mathcal{X} = (D_{i,j}^X, (\mu_i)_i)$ and $\mathcal{Y} = (D_{i,j}^Y, (\nu_j)_j)$, relaxation ρ , regularization ε

Output: approximation (π, γ) minimizing 6

- 1: Initialize matrix $\pi_{i,j} = \gamma_{i,j} = \mu_i \nu_j / \sqrt{(\sum_i \mu_i)(\sum_j \nu_j)}$, vector $g_j^{(s=0)} = 0$.
 - 2: **while** π has not converged **do**
 - 3: Update $\pi \leftarrow \gamma$
 - 4: Define $m(\pi) \leftarrow \sum_{i,j} \pi_{i,j}$, $\tilde{\rho} \leftarrow m(\pi)\rho$, $\tilde{\varepsilon} \leftarrow m(\pi)\varepsilon$
 - 5: Define $c \leftarrow \text{ComputeCost}(\mathcal{X}, \mathcal{Y}, \pi, \rho, \varepsilon)$
 - 6: **while** (f, g) has not converged **do**
 - 7: $f \leftarrow -\frac{\tilde{\varepsilon}\tilde{\rho}}{\tilde{\varepsilon}+\tilde{\rho}} \log \left[\sum_j \exp \left((g_j - c_{i,j}) / \tilde{\varepsilon} + \log \nu_j \right) \right]$
 - 8: $g \leftarrow -\frac{\tilde{\varepsilon}\tilde{\rho}}{\tilde{\varepsilon}+\tilde{\rho}} \log \left[\sum_i \exp \left((f_i - c_{i,j}) / \tilde{\varepsilon} + \log \mu_i \right) \right]$
 - 9: **end while**
 - 10: Update $\gamma_{i,j} \leftarrow \exp \left[(f_i + g_j - c_{i,j}) / \tilde{\varepsilon} \right] \mu_i \nu_j$
 - 11: Rescale $\gamma \leftarrow \sqrt{m(\pi)/m(\gamma)}\gamma$
 - 12: **end while**
 - 13: Return (π, γ) .
-

The functional \mathcal{L} now reads in this discrete setting

$$\int (d_X(x, x') - d_Y(y, y'))^2 d\pi(x, y) d\pi(x', y') = \sum_{i,j,k,\ell} (D_{i,j}^X - D_{k,\ell}^Y)^2 \pi_{i,k} \pi_{j,\ell},$$

$$\begin{aligned} \text{and } \text{KL}(\pi_1 \otimes \pi_1 | \mu \otimes \mu) &= \sum_{i,j} \log \left(\frac{\pi_{1,i} \pi_{1,j}}{\mu_i \mu_j} \right) \pi_{1,i} \pi_{1,j} - \sum_{i,j} \pi_{1,i} \pi_{1,j} + \sum_{i,j} \mu_i \mu_j \\ &= 2m(\pi) \sum_i \log \left(\frac{\pi_{1,i}}{\mu_i} \right) \pi_{1,i} - m(\pi)^2 + m(\mu)^2, \end{aligned}$$

where we define the marginals $\pi_{1,k} \triangleq \sum_j \pi_{k,j}$, $\pi_{2,\ell} \triangleq \sum_i \pi_{i,\ell}$ and $m(\pi) = \sum_{i,j} \pi_{i,j}$.

When one runs the stabilized implementation of Sinkhorn's iterations with a ground cost $C_{i,j} = C(x_i, y_j)$ between the points, it is necessary to use a Log-Sum-Exp reduction which reads

$$f_i \leftarrow -\frac{\varepsilon\rho}{\varepsilon + \rho} \text{LSE}_j \left[(g_j - C_{i,j}) / \varepsilon + \log(\mu_j) \right] \quad (31)$$

where LSE_j is a reduction performed on the index j . It reads

$$\text{LSE}_j(C_{i,j}) \triangleq \log \left(\sum_j \exp(C_{i,j} - \max_k C_{i,k}) \right) + \max_k C_{i,k}, \quad (32)$$

where the logarithm and exponential are pointwise operations.

We also provide an algorithm that computes the cost c_π^ε defined in Proposition (10). We focus on the case $D_\varphi = \rho \text{KL}$ and $\lambda(t) = t^2$ which is computable with complexity $O(n^3)$ as shown in Peyré et al. [2016]. Indeed, note that one has

$$\begin{aligned} \int (d_X(x, x') - d_Y(y, y'))^2 d\pi(x', y') &= \int d_X(x, x')^2 d\pi_1(x') + \int d_Y(y, y')^2 d\pi_2(y') \\ &\quad - 2 \int d_X(x, x') d_Y(y, y') d\pi(x', y'). \end{aligned}$$

Algorithm 3 – ComputeCost($\mathcal{X}, \mathcal{Y}, \pi, \rho, \varepsilon$) in discrete form

Input: mm-spaces $\mathcal{X} = (D_{i,j}^X, (\mu_i)_i)$ and $\mathcal{Y} = (D_{k,\ell}^Y, (\nu_j)_j)$, transport matrix $(\pi_{j,k})_{j,k}$, relaxation ρ , regularization ε

Output: cost c_{π}^{ε} defined in Proposition 10

- 1: Compute $\pi_{1,j} \leftarrow \sum_k \pi_{j,k}$ and $\pi_{2,k} \leftarrow \sum_j \pi_{j,k}$ $\{\pi_1 = \pi \mathbf{1}$ and $\pi_2 = \pi^\top \mathbf{1}\}$
 - 2: Compute $A_i \leftarrow \sum_j (D_{i,j}^X)^2 \pi_{1,j}$ $\{A = (D^X)^{\circ 2} \pi_1\}$
 - 3: Compute $B_\ell \leftarrow \sum_k (D_{k,\ell}^Y)^2 \pi_{2,k}$ $\{B = (D^Y)^{\circ 2} \pi_2\}$
 - 4: Compute $C_{i,\ell} \leftarrow \sum_j D_{i,j}^X (\sum_k D_{k,\ell}^Y \pi_{j,k})$ $\{C = D^X \pi D^Y\}$
 - 5: Compute $E \leftarrow \rho \sum_j \log \left(\frac{\pi_{1,j}}{\mu_j} \right) \pi_{1,j} + \rho \sum_k \log \left(\frac{\pi_{2,k}}{\nu_k} \right) \pi_{2,k} + \varepsilon \sum_{j,k} \log \left(\frac{\pi_{j,k}}{\mu_j \nu_k} \right) \pi_{j,k}$
 - 6: Return $c_{\pi,i,\ell}^{\varepsilon} \leftarrow A_i + B_\ell - 2C_{i,\ell} + E$
-

E Supplementary experiments

We provide in this section details on Section 4. We start with supplementary synthetic experiments illustrating various features of UGW. We present our approach to approximate the distance CGW using a bi-convex relaxation and alternate minimization. We prove the tightness of this relaxation and provide details on the experiments of Section 3. Then we provide details on the PU learning experiments.

E.1 Synthetic experiments

Robustness to outlier Figure 4 shows another experiment on a 2-D dataset, using the same display convention as in Figure 1. It corresponds to the two moons dataset with additional outliers (displayed in cyan). Decreasing the value of ρ (thus allowing for more mass creation/destruction in place of transportation) is able to reduce and even remove the influence of the outliers, as expected. Furthermore, using small values of ρ tends to favor “local structures”, which is a behavior quite different from UW (1). Indeed, for UW, $\rho \rightarrow 0$ sets to zero all the mass of π outside of the diagonal (points are not transported), while for UGW, it is rather pairs of points with dissimilar pairwise distances which cannot be transported together.

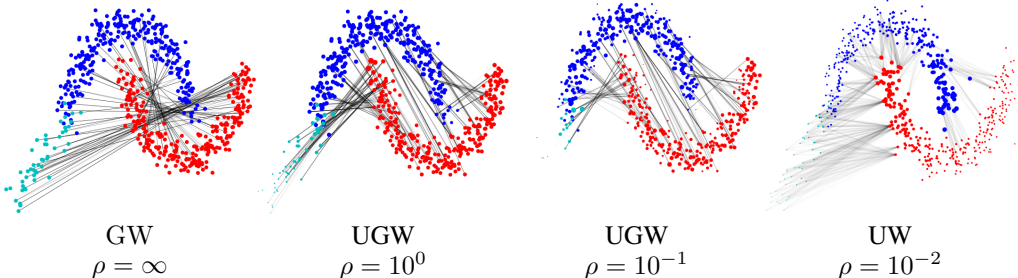


Figure 4: GW and UGW applied to two moons with outliers. A matching using UW is provided to display how invariance to isometries is encoded in the matching.

Graph matching and comparison with Partial-GW. We now consider two graphs (X, Y) equipped with their respective geodesic distances. These graphs correspond to points embedded in \mathbb{R}^2 , and the length of the edges corresponds to their Euclidean length. These two synthetic graphs are close to be isometric, but differ by addition or modification of small sub-structures. The colors $c(x)$ are defined on the “source” graph X and are mapped by an optimal plan π on $y \in Y$ to a color $\frac{1}{\pi_1(y)} \int_X c(x) d\pi(x, y)$. This allows to visualize the matching induced by GW and UGW for a varying ρ , as displayed in Figure 5. The graphs for GW should be taken as reference since there is no mass creation. The POT library [Flamary and Courty, 2017] is used to compute GW.

For large values of ρ , UGW behaves similarly to GW, thus producing irregular matchings which do not preserve the overall geometry of the shapes. In sharp contrast, for smaller values of ρ (e.g. $\rho = 10^{-1}$), some fine scale structures (such as the target’s small circle) are discarded, and UGW is able to produce a meaningful partial matching of the graphs. For intermediate values ($\rho = 10^0$), we observe that the two branches and the blue cluster of the source are correctly matched to the target, while for GW the blue points are scattered because of the marginal constraint.

Figure 6 shows a comparison with Partial-GW [Chapel et al., 2020], computed using the POT library. It is close to UGW with a TV^\otimes penalty, since partial OT is equivalent to the use of a TV relaxation of the marginal. UGW with a KL^\otimes penalty is first computed for a given ρ , then the total mass m of the optimal plan is computed, and is used as a parameter for PGW which imposes this total mass as a constraint. Figure 5 and 6 display the transportation strategy associated to both methods. KL -UGW operates smooth transitions between transportation and creation of mass, while PGW either performs pure transportation or pure destruction/creation of mass. In Figure 6 nodes of the graphs are removed and thus ignored by the matching. Note also that since PGW is equivalent to solving GW on sub-graphs, the color distribution of GW and PGW are similar.

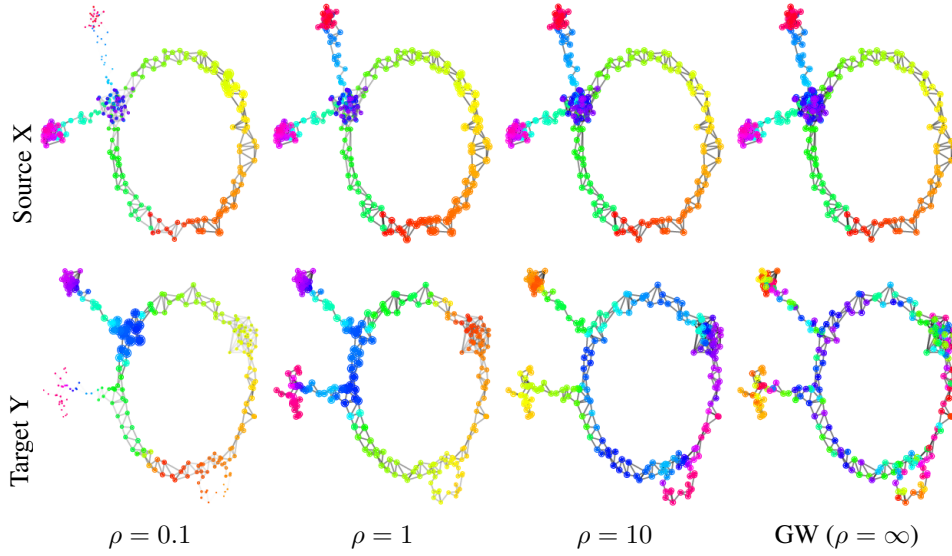


Figure 5: Comparison of UGW and GW for graph matching.

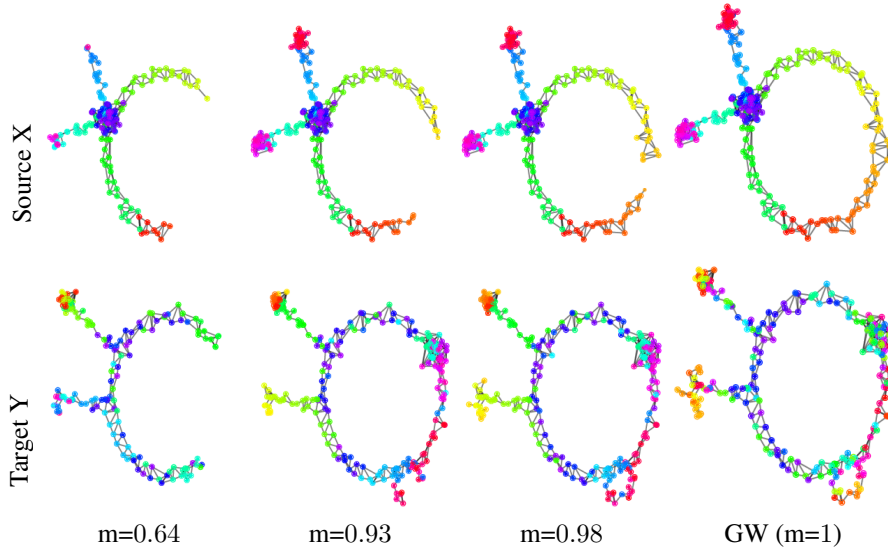


Figure 6: Comparison of Partial-GW for graph matching. Here m is the budget of transported mass.

Influence of ε . Figures 1, 4, 5 and 6 do not show the influence of ε . This parameter is set of a low value $\varepsilon = 10^{-2}$ on a domain $[0, 1]^2$ so as to approximate the optimal plan of the unregularized UGW problem. We present now an experiment on graphs which highlights the impact of (ε, ρ) on the plan π .

We compare two graphs $(\mathcal{X}, \mathcal{Y})$ displayed Figure 7. The graph \mathcal{X} is composed of two communities of equal size connected with random edges. The graph \mathcal{Y} is similar to \mathcal{X} , but the communities are imbalanced and it contains outliers. Moving inside a community costs 1, reaching another community costs 4 and reaching an outlier 2. We equip the mm-space with uniform weights and shortest path distance.

We plot in Figure 8 optimal transport plans π for given values of (ε, ρ) , including the balanced case GW_ε where $\rho = \infty$. The transport matrix has a block structure: the 2 horizontal blocks correspond to \mathcal{X} and its two communities, the 4 vertical blocks corresponds to \mathcal{Y} (with, from left to right, the large blue community, the small red one, then the pink and green outliers). Decreasing ρ results in a more structured transport matrix: outliers are removed and inter-community matching is avoided. Again,

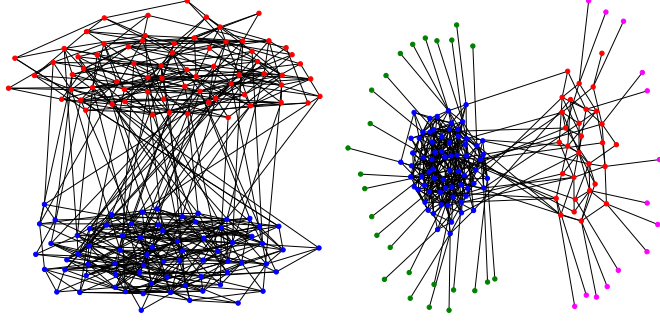


Figure 7: Graphs \mathcal{X} (left) and \mathcal{Y} (right) plotted using networkx.

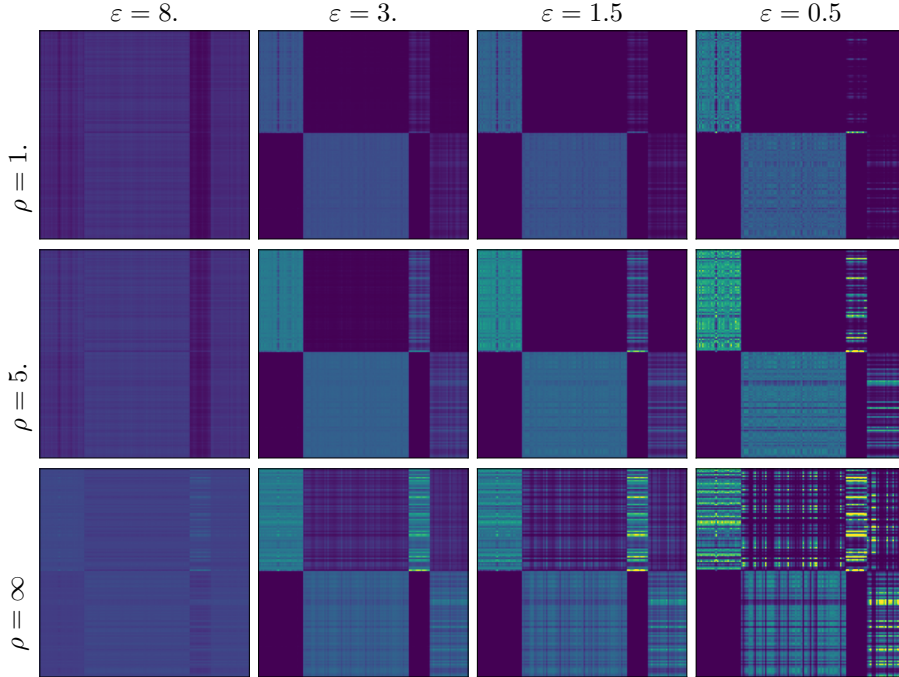


Figure 8: Display of the optimal transport plan π . The color scale is common to all plots.

the marginal constraint of GW_ε makes the plan more sensitive to structural noise (e.g. outliers) in graphs. Concerning the parameter ε , increasing it creates correlations between pairs of points whose distortion is of order of $\sqrt{\varepsilon}$. Indeed, we see for $\varepsilon = 3$ that correlation between communities and their outliers appear, even for small ρ . Furthermore, when ε is too large the transport becomes uninformative, which highlights a crucial trade-off between computational speed and expressiveness of the transport plan.

E.2 Computation of the CGW distance

In this section we focus on computing the distance CGW (4), which is a quadratic minimization program with linear constraint. Similar to what is performed with UGW 3, we consider a relaxation using a tensorized conic plan $\alpha \otimes \beta$ with $\alpha, \beta \in \mathcal{U}_p(\mu, \nu)$. The minimized cost thus reads

$$\mathcal{H}(\alpha, \beta) \triangleq \int \mathcal{D}([d_X(x, x'), rr'], [d_Y(y, y'), ss'])^q d\alpha([x, r], [y, s]) d\beta([x', r'], [y', s']). \quad (33)$$

Note that for fixed $\beta \in \mathcal{U}_p(\mu, \nu)$, the minimization w.r.t. α is a convex linear program with the linear conic constraint set $\mathcal{U}_p(\mu, \nu)$ and with cost

$$\mathcal{C}_{\mathcal{E}}(x, r, y, s) \triangleq \int \mathcal{D}([d_X(x, x'), rr'], [d_Y(y, y'), ss'])^q d\beta([x', r'], [y', s']). \quad (34)$$

Since we focus on the numerical implementation of CGW, we consider the setting of Gaussian-Hellinger distance which computes the distortion with $\lambda(t) = t^2$, due to a reduced memory and computation complexity to calculate $|d_X - d_Y|^2$ (see Section 3). In that case the cone distance reads for a given ρ

$$\mathcal{D}([d_X(x, x'), rr'], [d_Y(y, y'), ss'])^2 = \rho \left[(rr')^2 + (ss')^2 - 2rr'ss' e^{-|d_X - d_Y|^2/2\rho} \right]. \quad (35)$$

Before focusing on the discretization of this problem to make it computable, we prove that when $|d_X - d_Y|^2$ is a conditionally definite kernel then the above cost is a negative kernel on $\mathcal{U}_p(\mu, \nu)$. Thus Theorem 2 holds.

Proposition 11. *Assume that the kernel $|d_X - d_Y|^2$ is conditionally negative definite. Then the cost (35) is a negative definite kernel on $\mathcal{U}_p(\mu, \nu)$.*

Proof. Take any plan $\alpha \in \mathcal{U}_p(\mu, \nu)$. Integrating against $(rr')^2$ or $(ss')^2$ yields a constant term. Indeed one has for $(rr')^2$

$$\begin{aligned} \int (rr')^2 d\alpha([x, r], [y, s]) d\alpha([x', r'], [y', s']) &= \left(\int (r)^2 d\alpha([x, r], [y, s]) \right)^2 \\ &= \left(\int d\mu(x) \right)^2 \\ &= m(\mu)^2. \end{aligned}$$

Thus minimizing w.r.t. (35) is equivalent to minimizing w.r.t. $-2rr'ss' e^{-|d_X - d_Y|^2/2\rho}$, which is a product of positive definite kernels (rr') , (ss') and $e^{-|d_X - d_Y|^2/2\rho}$ thanks to Berg's Theorem Berg et al. [1984] and because we assume the kernel $|d_X - d_Y|^2$ is c.n.d. Due to the extra minus sign we get that the kernel is negative definite, which ends the proof. \square

An important point is to implement the constraint set $\mathcal{U}_p(\mu, \nu)$ which integrates against radial coordinates $(r, s) \in \mathbb{R}_+^2$. Such integration is impossible in practice, but thanks to Liero et al. [2015, Theorem 7.20], we know that the radius can be restricted to $[0, R]$ where $R^2 = m(\mu)^2 + m(\nu)^2$ (up to a dilation of the plan). Thus we propose to discretize the constraint by sampling regularly the interval as $\{lR/L, l \in \llbracket 0, L \rrbracket\}$.

We consider discrete mm-spaces as in Section D, i.e. mm-spaces noted as $\mathcal{X} = (D_{i,j}^X, (\mu_i)_i)$ and $\mathcal{Y} = (D_{i,j}^Y, (\nu_j)_j)$. Write a conic plan $\alpha_{ijkl} = \alpha([x_i, r_k], [y_j, s_l])$. The conic constraints read for $k \in \llbracket 0, K \rrbracket$ and $l \in \llbracket 0, L \rrbracket$

$$\sum_{j,k,l} \left(\frac{kR}{K} \right)^2 \alpha_{ijkl} = \mu_i \quad \text{and} \quad \sum_{i,k,l} \left(\frac{lR}{L} \right)^2 \alpha_{ijkl} = \nu_j.$$

The cost $\mathcal{C}_{\mathcal{E}}$ (34) is computed via the formula

$$\mathcal{C}_{ijkl} \triangleq \sum_{i',j',k',l'} \rho \left[\left(\frac{kR}{K} \frac{k'R}{K} \right)^2 + \left(\frac{lR}{L} \frac{l'R}{L} \right)^2 - 2 \left(\frac{kR}{K} \frac{k'R}{K} \frac{lR}{L} \frac{l'R}{L} \right) e^{-|D_{i,i'}^X - D_{j,j'}^Y|^2/2\rho} \right] \alpha_{i'j'k'l'}.$$

Eventually, the whole program solving one step of the alternate minimization algorithm is given Equation (36). The approximation of CGW is performed by alternatively updating α and $\mathcal{C}_{\mathcal{E}}$ until the minimization attains a local minima

$$\min_{\alpha_{ijkl}} \left\{ \sum_{i,j,k,l} \mathcal{C}_{ijkl} \alpha_{ijkl} \quad \text{s.t.} \quad \sum_{j,k,l} \left(\frac{kR}{K} \right)^2 \alpha_{ijkl} = \mu_i \quad \text{and} \quad \sum_{i,k,l} \left(\frac{lR}{L} \right)^2 \alpha_{ijkl} = \nu_j \right\}. \quad (36)$$

Dataset	# of samples	# of positives	Dim.	PCA Dim.
*-caltech	1,123	151	surf: 800 / decaf: 4096	surf: 10 / decaf: 40
*-amazon	958	92	surf: 800 / decaf: 4096	surf: 10 / decaf: 40
*-webcam	295	29	surf: 800 / decaf: 4096	surf: 10 / decaf: 40
*-dslr	157	12	surf: 800 / decaf: 4096	surf: 10 / decaf: 40

Table 2: Characteristics of datasets

Details on the experiments of Section 4. One can observe in the above procedure that the memory complexity of α and $\mathcal{C}_{\mathcal{E}}$ is prohibitively high to use it in practice, due to the discretization of the radial coordinate which make the size of both tensors scaling as $O(NMKL)$ where N, M are the number of samples in the spaces $(\mathcal{X}, \mathcal{Y})$. Thus our experiment are performed considering Euclidean mm-spaces composed of samples $N, M \in \{2, 3, 5\}$, and we take $K = L = 10$. To guarantee as much as possible that we reach the global minima, we consider 10 random initializations and 10 random permutation matrices P lifted as conic plan by setting $\alpha_{..kl} = P$ for any (k, l) . The latter initialization is assumed to be close to extremal points of the constraint polytope. Since Theorem 2 holds for Euclidean mm-spaces, the optimal plan is also an extremal point of the polytope. To compare CGW with UGW, we set a solver with a level of entropy $\varepsilon = 10^{-3}$. In Figure 3 we set $\rho = 10^{-1}$.

E.3 Details on PU learning experiments

Details on training for PU learning tasks. We present the characteristics of the datasets in Table 2. The variance of the accuracy results presented in Table 1 is presented in Table 4. The computations were made on an internal GPU cluster composed of 10 Tesla K80 and 3 Tesla P100. We also detail the parameters of the numerical solver computing UGW which is the core component of our numerical experiments.

- The maximum number of iteration to update the plan is set to 3000.
- The tolerance on convergence of π in log-scale is set to 10^{-5} , i.e. the algorithm stops when $\|\log \pi^{t+1} - \log \pi^t\|_{\infty} < tol$.
- The maximum number of iteration to update the Sinkhorn potentials is set to 3000.
- The tolerance on convergence of (f, g) is set to 10^{-6} , i.e. the algorithm stops when $\|f^{t+1} - f^t\|_{\infty} < tol$.

Initialization for cross-domain tasks. To initialize UGW when the features are different we propose to use a UOT solution of a matching between distance histograms which reads

$$\text{FLB}(\mathcal{X}, \mathcal{Y}) \triangleq \min \int_{X \times Y} |\bar{\mu} \star d_X - \bar{\nu} \star d_Y|^2 d\pi + \rho \text{KL}(\pi_1 | \mu) + \rho \text{KL}(\pi_2 | \nu) + \varepsilon \text{KL}(\pi | \mu \otimes \nu), \quad (37)$$

where $\mu \star d_X(x) \triangleq \int d_X(x, x') d\mu(x')$ is the eccentricity, i.e. a histogram of aggregated distances, and $\bar{\mu} = \mu/m(\mu)$. In Mémoli [2011] this relaxation is referred as FLB and is a lower bound of GW, but in our unbalanced setting this program cannot a priori be compared with UGW.

Reducing the number of parameters. In Table 1, the accuracy for UGW is performed by selecting a pair of parameters (ρ_1, ρ_2) for each task via a validation protocol detailed Section 4. It is desirable to reduce the number of parameters, to see if the performance does not significantly decrease, and avoid overparameterization of the task. We propose in this section two strategies. The first case keeps one pair (ρ_1, ρ_2) over all tasks. The second case keeps a pair for each pair of domain tasks (i.e. surf \leftrightarrow surf, decaf \leftrightarrow decaf, surf \leftrightarrow decaf and decaf \leftrightarrow surf) for a total of 8 parameters, which allows to normalize adaptively each dataset via an adapted choice of parameters (ρ_1, ρ_2) . The validation protocol is modified since we aggregate accuracies from different tasks. The selected parameters are obtained by taking the highest mean excess accuracy over all tasks, where the excess is defined by comparing the accuracy to the case where we only predict false positives. This measure of performance is computed on the validation folds, and we report the accuracy over the testing folds in Table 3.

Dataset	prior	Init (PW)	PGW	UGW	UGW (2 param.)	UGW (8 param.)
surf-C → surf-C	0.1	89.9	84.9	83.9	81.8	83.9
surf-C → surf-A	0.1	81.8	82.2	83.5	83.1	83.3
surf-C → surf-W	0.1	81.9	81.3	80.3	80.1	80.4
surf-C → surf-D	0.1	80.0	81.4	83.2	80.3	83.2
surf-C → surf-C	0.2	79.7	75.7	75.4	67.5	75.4
surf-C → surf-A	0.2	65.6	66.0	76.4	74.0	73.0
surf-C → surf-W	0.2	65.1	64.3	67.3	63.8	64.9
decaf-C → decaf-C	0.1	93.9	83.0	86.8	84.8	84.8
decaf-C → decaf-A	0.1	80.1	81.4	85.6	83.7	83.7
decaf-C → decaf-W	0.1	80.1	82.7	86.1	85.6	85.6
decaf-C → decaf-D	0.1	80.6	83.8	83.4	83.6	83.6
decaf-C → decaf-C	0.2	90.6	76.7	80.5	75.7	75.7
decaf-C → decaf-A	0.2	62.5	68.7	74.7	75.0	75.0
decaf-C → decaf-W	0.2	65.7	75.9	79.2	80.2	80.2

Dataset	prior	Init (FLB)	PGW	UGW	UGW (2 param.)	UGW (8 param.)
surf-C → decaf-C	0.1	85.0	85.1	85.6	85.0	85.0
surf-C → decaf-A	0.1	84.2	87.1	83.6	83.5	83.5
surf-C → decaf-W	0.1	86.2	88.6	86.8	87.4	87.4
surf-C → decaf-D	0.1	84.7	91.1	90.7	89.3	89.3
surf-C → decaf-C	0.2	74.8	75.6	75.9	76.2	76.2
surf-C → decaf-A	0.2	76.2	87.9	82.4	83.2	83.2
surf-C → decaf-W	0.2	81.5	88.4	89.9	88.8	88.8
decaf-C → surf-C	0.1	81.7	81.0	81.1	81.9	82.1
decaf-C → surf-A	0.1	80.9	81.2	82.4	81.2	82.1
decaf-C → surf-W	0.1	82.0	81.3	83.5	80.8	80.7
decaf-C → surf-D	0.1	80.0	80.8	81.5	80.0	81.5
decaf-C → surf-C	0.2	66.6	63.7	65.2	66.5	67.9
decaf-C → surf-A	0.2	62.9	62.4	69.3	62.2	68.5
decaf-C → surf-W	0.2	65.1	61.4	83.3	61.1	65.0

Table 3: Accuracy for all tasks. The left block are domain adaptation experiments with similar features, where both PGW and UGW are initialised with PW. The right block are domain adaptation experiments with different prior features, and the reported init is FLB (see Appendix E) used for UGW.

Dataset	prior	Init (PW)	PGW	UGW	UGW (2 param.)	UGW (8 param.)
surf-C → surf-C	0.1	2.05	1.95	2.93	2.14	2.94
surf-C → surf-A	0.1	1.25	1.89	2.14	2.29	3.33
surf-C → surf-W	0.1	1.33	1.82	0.73	0.45	0.82
surf-C → surf-D	0.1	0.00	1.69	2.63	0.73	2.63
surf-C → surf-C	0.2	2.98	4.66	5.07	2.42	5.07
surf-C → surf-A	0.2	2.87	3.29	3.59	2.15	9.46
surf-C → surf-W	0.2	1.95	2.12	9.22	1.82	7.61
decaf-C → decaf-C	0.1	1.61	2.24	2.46	1.64	1.64
decaf-C → decaf-A	0.1	0.44	1.91	4.52	2.08	2.08
decaf-C → decaf-W	0.1	0.44	2.55	1.65	1.90	1.90
decaf-C → decaf-D	0.1	0.92	1.54	2.06	1.67	1.67
decaf-C → decaf-C	0.2	2.54	3.59	5.73	2.53	2.54
decaf-C → decaf-A	0.2	2.09	4.39	7.46	4.52	4.52
decaf-C → decaf-W	0.2	1.93	3.60	5.89	3.61	3.61

Dataset	prior	Init (PW)	PGW	UGW	UGW (2 param.)	UGW (8 param.)
surf-C → decaf-C	0.1	2.79	2.64	3.01	2.71	2.71
surf-C → decaf-A	0.1	2.08	6.50	3.28	2.82	2.82
surf-C → decaf-W	0.1	1.89	5.63	3.97	3.62	3.62
surf-C → decaf-D	0.1	1.93	8.09	7.09	7.46	7.46
surf-C → decaf-C	0.2	2.56	3.32	4.02	3.66	3.66
surf-C → decaf-A	0.2	3.74	6.61	10.5	8.04	8.04
surf-C → decaf-W	0.2	2.75	5.82	3.33	3.64	3.64
decaf-C → surf-C	0.1	1.82	1.61	1.21	1.77	2.29
decaf-C → surf-A	0.1	1.18	1.94	2.11	1.36	2.10
decaf-C → surf-W	0.1	1.67	2.03	3.94	1.01	1.17
decaf-C → surf-D	0.1	0.00	1.60	1.70	0.00	1.70
decaf-C → surf-C	0.2	3.04	2.92	7.21	3.24	4.08
decaf-C → surf-A	0.2	1.84	4.54	5.92	2.04	5.19
decaf-C → surf-W	0.2	2.86	3.23	6.43	1.52	3.76

Table 4: Standard deviation of accuracy for all tasks of Figure 1. The left block are domain adaptation experiments with similar features, where both PGW and UGW are initialised with PW. The right block are domain adaptation experiments with different features, and the reported init is FLB (37) used for UGW.